

A Method for the Direct Measurement of the Force on a Satellite Due to Electromagnetic Radiation

LOUIS SICA

*Applied Optics Branch
Optical Sciences Division*

March 9, 1976



NAVAL RESEARCH LABORATORY
Washington, D.C.

Approved for public release; distribution unlimited.

UNCLASSIFIED

SECURITY CLASSIFICATION OF THIS PAGE (When Data Entered)

UNCLASSIFIED

REPORT DOCUMENTATION PAGE		READ INSTRUCTIONS BEFORE COMPLETING FORM	
1. REPORT NUMBER NRL Report 7961	2. GOVT ACCESSION NO.	3. RECIPIENT'S CATALOG NUMBER	
4. TITLE (and Subtitle) A METHOD FOR THE DIRECT MEASUREMENT OF THE FORCE ON A SATELLITE DUE TO ELECTRO-MAGNETIC RADIATION		5. TYPE OF REPORT & PERIOD COVERED Final report on an NRL problem	
		6. PERFORMING ORG. REPORT NUMBER	
7. AUTHOR(s) Louis Sica		8. CONTRACT OR GRANT NUMBER(s)	
9. PERFORMING ORGANIZATION NAME AND ADDRESS Naval Research Laboratory Washington, D.C. 20375		10. PROGRAM ELEMENT, PROJECT, TASK AREA & WORK UNIT NUMBERS NRL Problem N01-16.101 Project RR011 07 41 4807; Task Area RR0 110 741	
11. CONTROLLING OFFICE NAME AND ADDRESS		12. REPORT DATE March 9, 1976	
		13. NUMBER OF PAGES 46	
14. MONITORING AGENCY NAME & ADDRESS (if different from Controlling Office)		15. SECURITY CLASS. (of this report) Unclassified	
		15a. DECLASSIFICATION/DOWNGRADING SCHEDULE	
16. DISTRIBUTION STATEMENT (of this Report) Approved for public release; distribution unlimited			
17. DISTRIBUTION STATEMENT (of the abstract entered in Block 20, if different from Report)			
18. SUPPLEMENTARY NOTES			
19. KEY WORDS (Continue on reverse side if necessary and identify by block number)			
Coupled pendulum		Mechanical oscillator	
Force calibration		Radiation pressure	
Interferometer		Satellite deflection	
Mechanical common moding		Vibration isolation	
20. ABSTRACT (Continue on reverse side if necessary and identify by block number)			
<p>A technique was devised to measure the force on a satellite due to solar electromagnetic radiation pressure. The method consists of hanging the satellite as a pendulum and driving it on resonance with the light from a chopped solar simulator. From the measured amplitude of oscillation for a given number of cycles of driven motion, the driving force amplitude may be computed. The success of the method depends on the use of an optomechanical system which is insensitive to noise vibrations introduced at the pendulum pivot. The system consists of the satellite pendulum plus another pendulum of equal period and mass suspended from an upper</p> <p>(Continued)</p>			

DD FORM 1 JAN 73 1473

EDITION OF 1 NOV 65 IS OBSOLETE
S/N 0102-014-6601

i

UNCLASSIFIED

SECURITY CLASSIFICATION OF THIS PAGE (When Data Entered)

20. Abstract (Continued)

hanging platform. The relative coordinate of the satellite and its twin, which can be measured optically, is independent of the motion of the ceiling. Engineering tolerances for the optical and mechanical components of the device are treated in detail.

CONTENTS

INTRODUCTION	1
BASIC CONSIDERATIONS	1
THEORY	3
Motion of an Oscillator With Square-Wave Driving Force	3
Effect of Frequency Variation of Driving Force	7
Measurability of the Period of the Pendulum Oscillator	11
SIGNAL AND NOISE CONSIDERATIONS	13
Initial Deflection per Force Cycle in Satellite Case	13
Noise Measurement for Simulation Experiment	14
Deflection per Force Cycle in Proof-of-Principle Experiment	14
Noise Scaling	15
MECHANICAL METHOD TO IMPROVE SIGNAL-TO-NOISE RATIO	17
Simple Common-Mode Method	17
Common-Mode Method With Isolation	22
Additional Frequency-Matching Criterion	26
Time-Saving Method	29
Mechanical Requirements for Frequency Matching	29
OPTICAL MONITORING SYSTEM	31
Interferometer	31
Invariance Properties of Roof-Edge Reflectors	32
Pendulum Frequency-Tuning Monitor	38
RADIOMETER FORCE	39
SOLAR SIMULATION	40
CONCLUSION	40
ACKNOWLEDGMENT	40
REFERENCES	40
APPENDIX A — Derivation of Identities for Equations (5a) and (5b)	42

A METHOD FOR THE DIRECT MEASUREMENT OF THE FORCE ON A SATELLITE DUE TO ELECTROMAGNETIC RADIATION

INTRODUCTION

This report describes a proposed method for directly measuring the pressure of solar electromagnetic radiation on a satellite. There are indirect radiometric approaches to this problem, as well as the more direct method, explored here of measuring the mechanical response. The radiometric methods involve comprehensive data collection of such quantities as the angular distribution of radiation diffusely reflected from different satellite materials vs angle of incidence and wavelength. From the data collected and the solar spectral distribution, the force on a satellite could in principle be calculated on a computer, if the precise position of all surfaces were specified. The analysis of the errors and difficulties involved in such procedures is necessarily beyond the scope of this report. By reputation, the difficulties are formidable in cases where an accuracy of measurement of a few percent is the goal. Their careful appraisal would require another report as extensive as the present one.

The method explored here would yield the quantity sought directly from the data after a minor algebraic computation. It also allows a relatively simple cross check on its accuracy in that an object of simple shape having a mirror surface of known high reflectivity could be used in the measurement procedure. The measured force could then be compared with the value computed from momentum conservation. The price paid for these advantages is the requirement for a solar simulator large enough to irradiate the entire satellite cross section and a vacuum test chamber large enough to house both the satellite and simulator.

This report develops the radiation force measurement procedure as it would apply both to a laboratory proof-of-principle demonstration and to an actual satellite measurement. However, as data obtained on ambient vibration from preliminary laboratory measurements were only directly relevant to the proof-of-principle case, considerations pertaining to it are numerically somewhat more detailed than those pertaining to measurements on actual satellites.

BASIC CONSIDERATIONS

A description of the characteristics of the satellites to be calibrated is in order. The devices would weigh from 200 to 600 lb and would have a central metal body surrounded by several panels of solar cells which extend from it. The average diameter of the central body would be about 1 m, and each solar cell panel would extend outward about 1.25 m and be 0.5 m in width. The overall diameter of the device would then be greater than 3.5 m. The body itself might have a somewhat amorphous surface shape because of a metal foil heat shield and assorted fixtures. In general, the distribution of forces due to the light

pressure would be asymmetric, resulting in a torque as well as a translational force. The torque would be of no interest, however, and the measurement method should be unaffected by its existence when it occurred. It is desirable to perform the measurement in as short a time as possible, since the translational force must be measured for a large number of angular orientations of the device. The method of measurement should involve a laboratory procedure rather than measurements made on a satellite in orbit because perturbing forces other than radiation pressure jointly influence the orbital motion.

The method of measurement proposed to satisfy these requirements is to hang the satellite as a one-dimensional pendulum and drive it at the pendulum resonance frequency by chopping the output of a solar simulator. If the number of cycles of driven motion and the resulting amplitude of oscillation are measured, the magnitude of the driving force can be calculated from the solution to the equation of motion. The amplitude occurring after an infinite number of driving cycles is finite because of the presence of frictional forces. This limiting value for the amplitude is proportional to the driving force and inversely proportional to the product of the frequency and the dissipation constant. It follows that the observability of the driven oscillation depends ultimately on the magnitude of response of the oscillator to the ambient noise level. If its response to ambient noise is higher than the maximum amplitude of oscillation achievable for the driving force in question, the pendulum will have to be isolated from its noise environment before its response to the driving signal can be observed. Alternatively, it can be incorporated into a system arranged so that the vibrational noise affects both the satellite pendulum and its motion detector equally, allowing the noise to be subtracted out. This is the case when the detector is an interferometer in which the test arm measures the distance between two frequency-matched pendulums, one of which is the satellite and the other a dummy load of equal mass suspended so as to suffer the same perturbations. With such an arrangement, the noise will be automatically "common moded" out, and the signal-to-noise (S/N) ratio greatly increased.

In the following sections, the foregoing considerations will be developed in detail, and estimates will be made of the physical magnitudes and precision necessary for the successful realization of possible measurement options.

In the following section, expressions relating the square-wave driving-force amplitude, the displacement amplitude, and the number of cycles of driven motion are obtained together with the allowable mismatch between the drive and pendulum resonance frequencies for a given error resulting from the use of these expressions. Error magnitudes due to the effects of damping and of period variation with amplitude are then derived for the measurement of the pendulum resonance frequency. The fourth section deals with signal and noise levels based on estimates of the forces on a solar-illuminated satellite of typical dimensions and on a mirror illuminated by a 0.5-W laser beam, together with measurements of residual noise oscillations of a laboratory pendulum. The S/N ratio for a projected laboratory simulation of the method is found to be marginal. Mechanical common moding schemes to improve the S/N ratio are considered, as well as corresponding accuracy requirements on the pendulum lengths and temperatures, etc. Two optical monitoring systems are then described, one of which is suitable for the measurement of small amplitudes and the other for large amplitudes of oscillation. They correspond to the need to measure small relative pendulum displacements as well as pendulum frequencies at relatively large amplitudes above noise. Error limitations that may arise due to the existence of the radiometer force and to the existence of typical imperfections in solar simulation are dealt with briefly.

THEORY

Motion of an Oscillator With Square-Wave Driving Force

Although the expression for the amplitude of the damped harmonic oscillator driven by a sinusoidal driving force is well known, a square-wave driving force would probably be one's choice for use in an experiment. For a drive period of seconds, as would be necessary in the present case, given the physical dimensions of the satellite and consequent length of the pendulum, square-wave chopping of the light source could be accomplished with a mechanical shutter. Thus, the key theoretical result upon which the whole method rests is an expression for the displacement of the pendulum at the end of n cycles of the square-wave driving signal. This will now be derived, along with other closely related expressions of interest.

The differential equation of motion of a one-dimensional damped harmonic oscillator is [1]

$$m\ddot{x} + R\dot{x} + kx = F(t), \quad (1)$$

where m is the mass, R is a damping constant, k is a spring constant, $F(t)$ is the driving force, and x is the displacement of the oscillator. If the satellite is always illuminated from the same side, $F(t)$ is a square wave of amplitude F_0 which is nonnegative. The normalized force $f(t) = F(t)/F_0$ is shown in Fig. 1 with the switching times indicated. The solution to this equation can easily be expressed as an integral. Taking the Laplace transform of both sides of Eq. (1) for zero initial conditions and solving for the transformed displacement gives

$$\tilde{x}(s) = \frac{F_0}{m} \frac{\tilde{f}(s)}{\left(s^2 + \frac{2}{\tau}s + \omega_0^2\right)}, \quad (2)$$

where $2/\tau = R/m$, $\omega_0^2 = k/m$, F_0 is the magnitude of the driving force, and the tilde is used to indicate a Laplace transform.

Since the right-hand side of Eq. (2) consists of $\tilde{f}(s)$ multiplied by another factor, the convolution theorem may be applied to yield

$$x(t) = \frac{F_0}{\omega_1 m} \int_0^t e^{-\frac{(t-t')}{\tau}} \sin \omega_1(t-t') f(t') dt', \quad (3)$$

where

$$\omega_1 = \omega_0 \left(1 - \frac{1}{\tau^2 \omega_0^2}\right)^{1/2}.$$

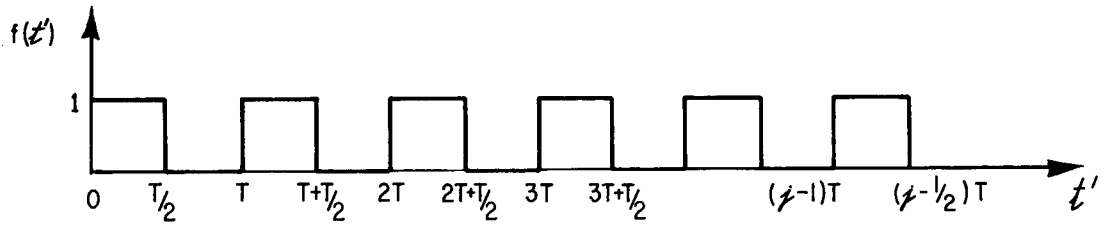


Fig. 1 — The normalized driving force on the satellite

The time t for which the value of the integral is desired is that at the end of the n th pulse of the light source, i.e. at $t = T(n - 1/2)$, where T is the period of the pulsed waveform. This value of $x(t)$ denoted by x_n can be written as a sum of integrals over those segments of the time domain in Fig. 1 for which $f(t')$ is not zero. Thus

$$x_n = \left(\frac{F_0}{\omega_1 m} \right) \sum_{j=1}^n I_j$$

where

$$I_j = \int_{(j-1)T}^{(j-1/2)T} e^{-(1/\tau)[(n-1/2)T - t']} \sin \omega_1 [(n-1/2)T - t'] dt'.$$

When the variable change $t'' = (n - 1/2)T - t'$ is made, this integral becomes

$$I_j = \int_{(n-j)T}^{(n-j+1/2)T} e^{-t''/\tau} \sin \omega_1 t'' dt''. \quad (4a)$$

The integration may be carried out directly, yielding

$$I_j = -\frac{1}{\left(\frac{1}{\tau^2} + \omega_1^2 \right)^{1/2}} \left\{ e^{(-T/\tau)(n-j+1/2)} \sin [\omega_1(n-j+1/2) + \xi] - e^{(T/\tau)(n-j)} \sin [\omega_1(n-j)T + \xi] \right\} \quad (4b)$$

where

$$\sin \zeta = \frac{\omega_1}{\left(\frac{1}{\tau^2} + \omega_1^2\right)^{1/2}}$$

and

$$\cos \zeta = \frac{\frac{1}{\tau}}{\left(\frac{1}{\tau^2} + \omega_1^2\right)^{1/2}} .$$

After summing the I_j as given in Eq. (4a), we obtain x_n in the form

$$x_n = \frac{F_0}{\omega_1 m} \frac{1}{\left(\frac{1}{\tau^2} + \omega_1^2\right)^{1/2}} \sum_{j=1}^n \left\{ e^{(-T/\tau)(n-j)} \sin [\omega_1(n-j)T + \zeta] \right. \\ \left. - e^{(-T/\tau)(n-j+1/2)} \sin [\omega_1(n-j+1/2)T + \zeta] \right\} .$$

When the summation index for fixed values of n is changed, this sum over j may be seen to be equal to the following sum over l ,

$$x_n = \frac{F_0}{\omega_1 m \left(\frac{1}{\tau^2} + \omega_1^2\right)^{1/2}} \sum_{l=0}^{n-1} \left\{ e^{-lT/\tau} \sin (\omega_1 l T + \zeta) \right. \\ \left. - e^{-(T/\tau)(l+1/2)} \sin [\omega_1(l+1/2)T + \zeta] \right\} . \quad (5a)$$

It is shown in Appendix A that

$$\sum_{l=0}^{n-1} e^{(-l/T)\tau} \sin(\omega_1 lT + \zeta) \equiv \Sigma_1 =$$

$$\cos \zeta \left\{ \frac{e^{-T/\tau_0} \sin \omega_1 T - e^{-T/\tau(n)} \sin \omega_1 Tn + e^{(-T/\tau)(n+1)} \sin \omega_1 T(n-1)}{1 - e^{-T/\tau} 2 \cos \omega_1 T + e^{-2T/\tau}} \right\}$$

$$+ \sin \zeta \left\{ \frac{1 - e^{-T/\tau} \cos \omega_1 T - e^{-T/\tau(n)} \cos \omega_1 Tn + e^{(-T/\tau)(n+1)} \cos \omega_1 T(n-1)}{1 - e^{-T/\tau} 2 \cos \omega_1 T + e^{-2T/\tau}} \right\} \quad (5b)$$

and

$$\sum_{l=0}^{n-1} e^{(-T/\tau)(l+1/2)} \sin[\omega_1(l+1/2)T + \zeta] \equiv \Sigma_2 =$$

$$e^{-T/2\tau} \cos\left(\frac{\omega_1 T}{2} + \zeta\right) \left\{ \frac{e^{-T/\tau} \sin \omega_1 T - e^{(-T/\tau)n} \sin \omega_1 Tn + e^{(-T/\tau)(n+1)} \sin \omega_1 T(n-1)}{1 - e^{-T/\tau} 2 \cos \omega_1 T + e^{-2T/\tau}} \right\}$$

$$+ e^{-T/2\tau} \sin\left(\frac{\omega_1 T}{2} + \zeta\right) \left\{ \frac{1 - e^{-T/\tau} \cos \omega_1 T - e^{(-T/\tau)n} \cos \omega_1 Tn + e^{(-T/\tau)(n+1)} \cos \omega_1 T(n-1)}{1 - e^{(-T/\tau)2} \cos \omega_1 T + e^{-2T/\tau}} \right\} \quad (5c)$$

In terms of Σ_1 and Σ_2 , Eq. (5a) may be written

$$x_n = \frac{F_0}{\omega_1 m} \frac{1}{\left(\frac{1}{\tau^2} + \omega_1^2\right)^{1/2}} (\Sigma_1 - \Sigma_2). \quad (5d)$$

A number of expressions of interest can now be calculated. First, one would like to know x_n when the fundamental frequency of the driving force is tuned to the resonance frequency

of the pendulum, i. e. to angular frequency ω_1 . This is the expression one would use in determining the force on a satellite from experimental data. In this case $\omega_1 T_1 = 2\pi$, and

$$x_n = \frac{F_0 (1 + e^{-T_1/2\tau}) (1 - e^{-T_1 n/\tau})}{m \left(\frac{1}{\tau^2} + \omega_1^2 \right) (1 - e^{-T_1/\tau})} \quad (6)$$

The maximum displacement amplitude obtainable at this frequency, the value at $n = \infty$, is

$$x_\infty(T_1) = \frac{F_0 (1 + e^{-T_1/2\tau})}{m \left(\frac{1}{\tau^2} + \omega_1^2 \right) (1 - e^{-T_1/\tau})} \quad (7)$$

Since in practical cases, $T_1/\tau \ll 1$, the exponential may be approximated by the first two terms of its power series expansion. This, plus the fact that $1/\tau^2 \ll \omega_1^2$, leads to the expression

$$x_\infty = \frac{2}{\pi} \frac{F_0}{\omega_1 R} = \frac{2F_0}{\omega_1^2 m} \frac{\tau}{T_1} \quad (8)$$

which except for the factor $2/\pi$, is the same as the amplitude at resonance in the case of a sinusoidal driving force.

Effect of Frequency Variation of Driving Force

It is necessary to know the shape of the response function for small departures of the driving period from T_1 in order to know how precisely the driving frequency must be determined if Eq. (7) is to be used for the computation of F_0 . This may be found with the aid of the expressions for Σ_1 and Σ_2 above, with n set equal to infinity. In this case,

$$\begin{aligned} \Sigma_1 - \Sigma_2 = & \frac{1}{(1 - e^{-T/\tau} 2 \cos \omega_1 T + e^{-2T/\tau}) \left(\frac{1}{\tau^2} + \omega_1^2 \right)^{1/2}} \left\{ \frac{1}{\tau} e^{-T/\tau} \sin \omega_1 T \right. \\ & - \sin \frac{\omega_1 T}{2} \left[\frac{e^{-T/2\tau} + e^{(-3/2)(T/\tau)}}{\tau} \right] - \omega_1 e^{-T/\tau} \cos \omega_1 T \\ & \left. + \omega_1 \cos \frac{\omega_1 T}{2} \left[e^{(-3/2)(T/\tau)} - e^{-T/2\tau} \right] + \omega_1 \right\} . \end{aligned}$$

We compute the value of this expression for $T = T_1 + \Delta T$. After simplifying, we obtain

$$\begin{aligned} \Sigma_1 - \Sigma_2 = & \frac{1}{\left(1 - e^{-T/\tau} 2 \cos \omega_1 \Delta T + e^{-2T/\tau}\right) \left(\frac{1}{\tau^2} + \omega_1^2\right)^{1/2}} \times \\ & \left\{ \frac{1}{\tau} e^{-T/\tau} \sin \omega_1 \Delta T + \sin \frac{\omega_1 \Delta T}{2} \left[\frac{e^{-T/2\tau} + e^{-(3/2)T/\tau}}{\tau} \right] \right. \\ & \left. - \omega_1 e^{-T/\tau} \cos \omega_1 \Delta T - \omega_1 \cos \frac{\omega_1 \Delta T}{2} \left[e^{-(3/2)(T/\tau)} - e^{-T/2\tau} \right] + \omega_1 \right\}. \quad (9a) \end{aligned}$$

The parenthesis in the denominator which contains the cosine term is of the resonance form for small ΔT . This may be shown by replacing the cosine by the first two terms of its power series expansion and obtaining the expression

$$1 - e^{-T/\tau} 2 \left(1 - \frac{1}{2} (\omega_1 \Delta T)^2\right) + e^{-2T/\tau}.$$

After rearranging terms, we have

$$(1 - e^{-T/\tau})^2 + (\omega_1 \Delta T)^2 e^{-T/\tau} \simeq \left(\frac{T}{\tau}\right)^2 + (\omega_1 \Delta T)^2, \quad (9b)$$

since for the systems of interest here, $T/\tau \ll 1$. Now, the trigonometric terms in the numerator of Eq. (9a) may be expanded to first order. This results in

$$\begin{aligned} & \frac{1}{\tau} e^{-T/\tau} \omega_1 \Delta T + \omega_1 \frac{\Delta T}{2} \left(\frac{e^{-(T/2\tau)} + e^{-(3/2)(T/\tau)}}{\tau} \right) - \omega_1 e^{-T/\tau} \\ & - \omega_1 (e^{-(3/2)(T/\tau)} - e^{-(T/2\tau)}) + \omega_1. \end{aligned}$$

If the exponentials are expanded in turn and if we again use the fact that T/τ is small, this may be reduced to

$$\frac{2\omega_1}{\tau} (\Delta T + T). \quad (9c)$$

Substituting expressions (9b) and (9c) into Eq. (9a) results in

$$\Sigma_1 - \Sigma_2 = \frac{2(\omega_1/\tau)(\Delta T + T)}{\left[\left(\frac{T}{\tau}\right)^2 + (\omega_1 \Delta T)^2\right] \left(\frac{1}{\tau^2} + \omega_1^2\right)^{1/2}} \quad (10)$$

After inserting the value given by Eq. (10) into Eq. (5c), we have

$$x_\infty(\Delta T) = \frac{2F_0(\Delta T + T)}{m\left(\frac{1}{\tau^2} + \omega_1^2\right)\tau \left[\left(\frac{T}{\tau}\right)^2 + (\omega_1 \Delta T)^2\right]}.$$

It may be observed that the maximum of this expression is offset slightly from $\Delta T = 0$ just as in the case of a purely sinusoidal driving force [1]. Nevertheless, ω_1 is a convenient angular frequency to measure and to use for driving the oscillator. Thus we normalize Eq. (10) to Eq. (8). After dividing the former by the latter and neglecting $1/\tau^2$ compared to ω_1^2 in Eq. (10), we obtain

$$\frac{x_\infty}{x_\infty(\Delta T=0)} = \frac{\left[\frac{\Delta T}{T} + 1\right]}{1 + \left(\tau\omega_1 \frac{\Delta T}{T}\right)^2} \quad (11)$$

In Eq. (11), T may now be replaced by T_1 , the difference between them being negligible to this order. One may now find the value of $\Delta T/T_1$, corresponding to a decrease in Eq. (11) from unity to 0.99. Solving the equation $x_\infty/x_\infty(\Delta T=0) = 0.99$, we find that

$$\left|\frac{\Delta T}{T_1}\right| = \frac{1}{10\tau\omega_1} \quad (12)$$

This is the same estimate that one gets by neglecting the $\Delta T/T$ in the numerator of Eq. (11) at the outset, indicating that the shift of the actual peak of the response from the frequency ω_1 is negligible in the present context.

Equation (12) is a worst-case estimate of the accuracy of the driving frequency necessary for the use of the on-resonance equations. Since the damping times for situations of interest are of the order of many minutes or hours, it would be unfortunate if it were necessary to drive the pendulum into the saturation region in order to obtain a sufficient S/N ratio for the measurement. The most desirable situation would be one in which the system gave a measurable response after a driving time short compared to the transient response time of the pendulum.

To obtain an estimate of the necessary accuracy of the driving frequency for this case, we must start again from Eqs. (5). For the case we are considering, $lT \ll \tau$, so the exponentials may be ignored in Σ_1 and Σ_2 . Under this condition, we obtain [2]

$$\Sigma_1 = \sum_{l=0}^{n-1} \sin(\omega_1 lT + \zeta) = \sin\left(\zeta + \frac{n-1}{2} \omega_1 T\right) \frac{\sin \frac{n}{2} \omega_1 T}{\sin \frac{\omega_1 T}{2}}$$

and

$$\Sigma_2 = \sum_{l=0}^{n-1} \sin\left[\omega_1 lT + \left(\frac{\omega_1 T}{2} + \zeta\right)\right] = \sin\left(\frac{\omega_1 T}{2} + \zeta + \frac{n-1}{2} \omega_1 T\right) \frac{\sin \frac{n\omega_1 T}{2}}{\sin \frac{\omega_1 T}{2}}.$$

From these expressions we obtain

$$\Sigma_1 - \Sigma_2 = \frac{-2 \sin \frac{n\omega_1 T}{2}}{\sin \frac{\omega_1 T}{2}} \sin \frac{\omega_1 T}{4} \cos\left[\zeta + \left(n - \frac{1}{2}\right) \frac{\omega_1 T}{2}\right].$$

Substituting $T = T_1 + \Delta T$ yields

$$\begin{aligned} \Sigma_1 - \Sigma_2 = & \frac{2 \sin \frac{n\omega_1 \Delta T}{2} \cos \frac{\omega_1 \Delta T}{4}}{\left(\frac{1}{\tau^2} + \omega_1^2\right)^{1/2} \sin \frac{\omega_1 \Delta T}{2}} \left\{ \omega_1 \cos\left[\left(n - \frac{1}{2}\right) \omega_1 \frac{\Delta T}{2}\right] \right. \\ & \left. + \frac{1}{\tau} \sin\left[\left(n - \frac{1}{2}\right) \omega_1 \frac{\Delta T}{2}\right] \right\}. \end{aligned}$$

Neglecting terms of the order of $1/\tau$ and $1/\tau^2$, we obtain after some further simplification,

$$\Sigma_1 - \Sigma_2 = \frac{\sin n\omega_1 \Delta T}{\sin \frac{\omega_1 \Delta T}{2}} \cos^2 \frac{\omega_1 \Delta T}{4}.$$

Since we are interested in the behavior of this expression for small values of ΔT , we set the cosine-squared factor equal to one and have for x_n ,

$$x_n = \frac{2F_0 n}{m\omega_1^2} \left(\frac{\sin n\omega_1 \Delta T}{n\omega_1 \Delta T} \right). \quad (13)$$

From Eq. (13), we can obtain two results of interest, the value of x_n for driving precisely on resonance ($\Delta T = 0$) and the frequency accuracy required of the driving apparatus. It is clear from the behavior of the $(\sin x)/x$ factor in Eq. (13) that to maintain the same error size as n becomes larger, ΔT must be made smaller. In particular, for an error of 1%, and after replacing $\sin(n\omega_1 \Delta T)$ by the first two terms of its power series expansion, we have

$$1 - \frac{1}{6} (n\omega_1 \Delta T)^2 = 1 - 0.01.$$

Solving for $\Delta T/T$ results in

$$\frac{\Delta T}{T} \approx \frac{4 \times 10^{-2}}{4} = \frac{1}{2.5 \times 10n}. \quad (14)$$

This value for $\Delta T/T$ may be considerably larger than the value given by Eq. (12). The fact that the necessary accuracy of the driving frequency changes with the length of the driving time is physically consistent with the fact that time and frequency are conjugate variables in Fourier analysis.

Measurability of the Period of the Pendulum Oscillator

In order to match the drive frequency to a given oscillator frequency, we must first measure the oscillator frequency. If a pendulum is set in motion by some disturbing impulse at $t = 0$, the frequency ω_1 may be determined by monitoring the motion. It follows immediately from Eq. (3) that the motion of a pendulum after such an impulse is given by

$$x(t) = \frac{F_0}{\omega_1 m} e^{-t/\tau} \sin \frac{2\pi t}{T_1}. \quad (15)$$

If the time between two successive excursions to a small fraction ϵ of the initial amplitude is measured, the period T_1 is obtained along with a small error from the slow exponential decay of the oscillation. It is necessary to estimate the magnitude of this error, since it effectively limits the accuracy with which the drive frequency can be set equal to ω_1 .

On two successive cycles, Eq. (15) gives

$$\frac{F_0}{\omega_1 m} \exp\left(\frac{-nT_1 + \delta t_n}{\tau}\right) \sin \frac{2\pi}{T_1} (nT_1 + \delta t_n) = \frac{F_0}{\omega_1 m} \epsilon$$

and

$$\frac{F_0}{\omega_1 m} \exp\left(\frac{-(n+1)T_1 + \delta t_{n+1}}{\tau}\right) \sin \frac{2\pi}{T_1} [(n+1)T_1 + \delta t_{n+1}] = \frac{F_0}{\omega_1 m} \epsilon,$$

with the time between observations given by $T_{\text{obs}} = T_1 + \delta t_{n+1} - \delta t_n$. These equations can immediately be put in the form

$$\exp\left(\frac{-\delta t_n}{\tau}\right) \sin \frac{2\pi \delta t_n}{T_1} = \epsilon e \frac{nT_1}{\tau}$$

and

$$\exp\left(\frac{-\delta t_{n+1}}{\tau}\right) \sin \frac{2\pi \delta t_{n+1}}{T_1} = \epsilon \exp\left[\frac{(n+1)T_1}{\tau}\right].$$

We assume that the measurements are made soon after the pendulum is set in motion, so that $nT_1/\tau \ll 1$. Expanding the sines and exponentials in power series, keeping only terms which are of first order in δt , and subtracting the $(n+1)$ th from the n th equation leads to the result

$$\frac{\Delta T_1}{T_1} \equiv \frac{\delta t_{n+1} - \delta t_n}{T_1} = \frac{\epsilon}{2\pi} \frac{T_1}{\tau}. \quad (16)$$

Along the same lines, it must be considered that even in the absence of damping, the pendulum is only approximately a simple harmonic oscillator. The intrinsic variation of its frequency with amplitude must be examined over the range of amplitudes of interest. It is shown in standard mechanics texts [1] that the period of a simple pendulum is given by

$$T = \frac{4}{\omega_0} \int_0^{\pi/2} \frac{d\phi}{(1 - k^2 \sin^2 \phi)^{1/2}},$$

where $k = \sin \theta_0/2$, θ_0 is the angular amplitude of oscillation measured from the vertical, and the angular frequency ω_0 is the frequency of the pendulum for vanishingly small amplitudes of oscillation. Since k is very small in the present application, the square root may

be approximated by using the binominal expansion and keeping only the first term. Thus,

$$T \approx \frac{4}{\omega_0} \int_0^{\pi/2} \left(1 + \frac{1}{2} k^2 \sin^2 \phi \right) d\phi.$$

This may be immediately integrated to yield

$$\frac{T - T_0}{T_0} = \frac{k^2}{4}. \quad (17)$$

SIGNAL AND NOISE CONSIDERATIONS

Initial Deflection per Force Cycle in Satellite Case

The pressure exerted by a parallel beam of light on a totally absorbing surface oriented so that it is normal to the beam is equal to the energy per unit volume ρ of the incident radiation [3]. In turn,

$$\rho = \frac{W}{c} \quad (18)$$

where W is the number of watts per square meter in the incident radiation and c is the speed of light. To estimate the magnitude of the force due to the radiation pressure of sunlight on the surface of a satellite requires that a value of 800 W/m^2 be used† for the irradiance. The resulting pressure is $2.6 \times 10^{-6} \text{ N/m}^2$. The satellite is assumed to consist of a central body plus two or more panels extending outward from it. The total area presented to the incident solar radiation is assumed to be 4 m^2 . Since we are interested in orders of magnitude, the area could be increased by a factor of two or three without qualitatively changing the results. From the above figures, the force on the satellite is $F = \rho A = 10.9 \times 10^{-6} \text{ N}$. From Eq. (13), with ΔT set equal to zero, the amplitude of oscillation vs the number of driving cycles may be computed. A mass of 600 lb (272.2 kg) is taken as a representative value. If the pendulum is 4 m long, its period is 4 sec and the angular frequency is $\pi/2$. With these values,

$$x_n = 3.24 \times 10^{-2} n \text{ } \mu\text{m}, \quad (19a)$$

where n denotes the number of driven cycles of oscillation. It is interesting to measure this deflection in terms of the wavelength of He-Ne laser light at $0.6328 \text{ } \mu\text{m}$. The result is

$$x_n / \lambda_{6328} = 5.1 \times 10^{-2} n. \quad (19b)$$

†The solar constant or the power per unit area at normal incidence at the top of the atmosphere is about 1400 W/m^2 and is constant to 3.5%. The distinction for the estimates made herein is slight.

The ease or difficulty in detecting a pendulum displacement amplitude of this order of magnitude depends on its residual noise oscillation, which in turn results from the vibrational noise in its environment.

Noise Measurement for Simulation Experiment

To get some idea of the order of magnitude of the noise to be expected, at least in a simulation experiment, we carried out a preliminary measurement. A small pendulum was suspended from the end of a vibration isolation table and its period, damping time, and residual noise oscillation were measured. The motion of the pendulum was monitored using moire fringes from two 39.37-cycle/cm Ronchi rulings imaged one upon the other at unit magnification. The gratings, one attached to the pendulum and the other stationary, were illuminated by a 5-mW He-Ne laser beam. When the pendulum was set into oscillation, its changes in position resulted in changes in transmission of the Ronchi ruling pair. These transmission changes were monitored with the aid of a pin-diode detector and oscilloscope.

Two pendulum bobs were used, a heavy bob consisting of a lead brick (10.4×10^3 g), and a light bob made of aluminum (92.6 g). The decay constant for the heavy bob was 6.5×10^3 sec, whereas that for the light bob was 750 sec. The lengthening of the decay time with increasing mass is not unexpected, since $1/\tau = R/2m$. (One would intuitively expect the dependence of R on m to be weak enough so that τ increases with increasing m . R for the large mass was 10 times greater than for the small mass, so that the expectation was fulfilled.) The residual motion of the heavy pendulum was approximately $10 \mu m$ peak to peak, while for the light pendulum it varied from 3 to $11 \mu m$ peak to peak. Qualitatively, the pendulums appeared to respond to vibrations associated with events such as people walking in the halls, doors slamming, etc. When the amplitude of oscillation had reached a minimum level, an event of this type seemed to precede an increase in its magnitude.

It is useful to consider the implications of the above laboratory noise observations for a simulation experiment of the whole satellite calibration scheme. Having a miniaturized laboratory version of the procedure would be most desirable, to provide a proof-of-principle demonstration of the method before going to the expense of acquiring a solar simulator.

Deflection per Force Cycle in Proof-of-Principle Experiment

In a laboratory proof-of-principle experiment, an argon laser could be used to drive a small laser cavity end mirror mounted on a pendulum platform. Because of the low heating which would occur in the case of a low-loss mirror, the experiment would appear to be feasible in air if well shielded from drafts.

The force on the reflector would be the integral of the pressure exerted by each element of the beam-intensity profile, or

$$F = \frac{1}{c} \int w(x, y) dx dy = \frac{P}{c}, \quad (20)$$

where P is the total power in the beam. In addition, for a reflector, the result needs to be multiplied by a factor of 2 as compared to an absorber. Thus, in the case of a 1/2-W laser, the force would be

$$F = 3.3 \times 10^{-9} N.$$

Assuming a pendulum mass of 0.4 kg and a period of 1 sec, one finds from Eq. (13) that

$$x_n = 0.4 \times 10^{-3} n \mu m \quad (21a)$$

or

$$\frac{x_n}{\lambda_{6328}} = 6.6 \times 10^{-4} n. \quad (21b)$$

Since this expression is much smaller than the noise residual oscillation measured for reasonable values of n (less than 100), the maximum possible amplitude of oscillation for the given force must be inquired about. This may be computed from Eq. (8) if R is known. The value of R obtained for the small pendulum used in the preliminary experiment will be used for the estimate, even though its mass was 0.1 kg rather than 0.4 kg as in the present case. The value of R obtained was $R = 1.38 \times 10^{-4}$ kg/sec. With this value, $x = 2.42 \mu m$. Thus, a S/N ratio of somewhat less than 1 may be achieved after the transient dies out, or after about 50 min. This is clearly a very unfavorable result. A method for dealing with this problem will be discussed in the next section. We will finish this section with the development of a noise scaling relation.

Noise Scaling

Every environment is unique in its generation of vibrational and acoustic disturbances. Further, the response of a pendulum to a noise environment depends on its physical characteristics as an oscillator. Thus, the observations made with a pendulum of a given mass, frequency, and damping time on a vibration isolation table in a laboratory are not necessarily representative of those that would be made with a pendulum of different characteristics located in a large environmental test chamber. To connect the latter with the former, a scaling law is necessary in addition to measurements of the important noise parameters. There are two limiting forms of scaling law which may be derived. One corresponds to the situation in which the noise bandwidth is much narrower than the oscillator bandwidth, i. e., the pendulum is driven by a sinusoidal driving force. This case is trivial and immediately follows from the equation of motion. The second case is that in which the bandwidth of the noise is much broader than that of the pendulum. The scaling law for this case may be derived as follows.

We write Eq. (1) in terms of its Fourier transform to obtain

$$\int_0^{\infty} \hat{x}_T \left(-4\pi^2 \nu^2 + \frac{R}{m} 2\pi i \nu + 4\pi^2 \nu_0^2 \right) e^{2\pi i \nu t} d\nu = \frac{1}{m} \int_0^{\infty} f_T(\nu) e^{2\pi i \nu t} d\nu,$$

where the T subscript on x and f indicates truncation of the respective functions outside of the time interval $-T$ to $+T$. The caret over the x indicates the Fourier transform. From this it follows that

$$\hat{x}_T(\nu) = \frac{1}{m} \frac{f_T(\nu)}{\left[4\pi^2(\nu_0^2 - \nu^2) + \frac{R}{m} 2\pi i\nu \right]}.$$

Using Parseval's theorem, we obtain

$$\int_{-T}^T \frac{\overline{x_T^\tau(t)^2}}{2T} dt = 2 \int_0^\infty \frac{\overline{\hat{x}_T(\nu)\hat{x}_T(\nu)^2}}{2T} d\nu = 2 \int_0^\infty \frac{\overline{|f_T(\nu)|^2}}{2Tm^2 \left[(\omega_0^2 - \omega^2)^2 + \left(\frac{R}{m} \omega\right)^2 \right]},$$

where the bar above the integrand indicates the ensemble average. The limit as $T \rightarrow \infty$ yields the mean square oscillation due to the noise driving force. Thus,

$$\overline{x_N^2} = \frac{|f_N|^2}{m^2\pi} \int_0^\infty \frac{d\omega}{(\omega_0^2 - \omega^2)^2 + \left(\frac{R}{m} \omega\right)^2},$$

where $|f_N|^2$ is the infinite time ensemble average of the noise power density assumed white over the bandwidth of the oscillator. The integration over ω may be performed to yield $\pi m/2R\omega_0^2$. The final value for the *rms* noise is thus

$$\sqrt{\overline{x_N^2}} = \frac{|f_N|}{\sqrt{2mR} \omega_0}. \quad (22)$$

Note that, in the case of noise introduced by pivot vibration, $|f_N| = m\omega_0^2|\xi_0|$ where $|\xi_0|$ is the ensemble-averaged pivot amplitude. The complex oscillator response to a sinusoidal signal of amplitude f_s at angular resonance frequency ω_0 is $x_s = f_s/R\omega_0 j$, which leads to an *rms* value for the signal response of

$$\sqrt{\overline{x_s^2}} = \frac{1}{\sqrt{2}} \frac{f_s}{R\omega_0}. \quad (23)$$

The S/N ratio is thus

$$\frac{\sqrt{\overline{x_s^2}}}{\sqrt{\overline{x_N^2}}} = \frac{f_s}{f_N \sqrt{\frac{R}{m}}} = \frac{f_s}{f_N} \sqrt{\frac{\tau}{2}} = \frac{f_s}{\xi_0 \omega_0^2 \sqrt{mR}}. \quad (24)$$

Unfortunately, since R may depend on m , these formulas must be used with caution.

MECHANICAL METHOD TO IMPROVE SIGNAL-TO-NOISE RATIO

Simple Common-Mode Method

The various aspects of pendulum response, S/N ratio, etc., have been treated as though the pendulum were constrained to move in one dimension only. An arrangement of the pendulum supporting wires which results in such constraint is drawn in Fig. 2. Shown is a five-stranded support system, arranged so as to provide a three-point suspension. In each of two pairs of two strands, the strands meet at a point at the platform with a large angle between them. The two support V's arranged in this way lie in parallel planes. The third support point is held by a single vertical strand which lies in a plane parallel to the other support planes. The pendulum can only move in a circle which lies in a plane perpendicular to the support planes. An added benefit of this arrangement is that there is no rotation of the pendulum about an axis through its center of mass. The only motion allowed is pure translation in a vertical circle. Since the amplitude of oscillation being considered here is very small, the first-order approximation to linear motion is a very good one.

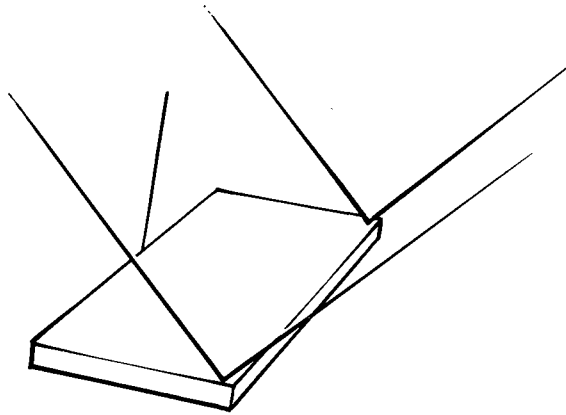


Fig. 2 — Five-stranded support system to constrain pendulum to motion in a plane [4]

The linear motion allows consideration of a mechanical noise-reduction method as follows. Consider two pendulums suspended from a rigid though movable (due to noise) support plane as shown in Fig. 3. The ξ coordinate indicates the horizontal displacement of the support plane with respect to a Newtonian coordinate system. The coordinates x_1 and x_2 indicate horizontal displacements of masses m_1 and m_2 from a vertical line fixed with respect to the upper support plane. The position of either mass with respect to the Newtonian coordinate system is $x_i + \xi$, where $i = 1, 2$.

Velocity-dependent damping forces of two kinds are assumed. They consist of internal friction in the support wires, and air friction if the system is not in vacuum. For a system

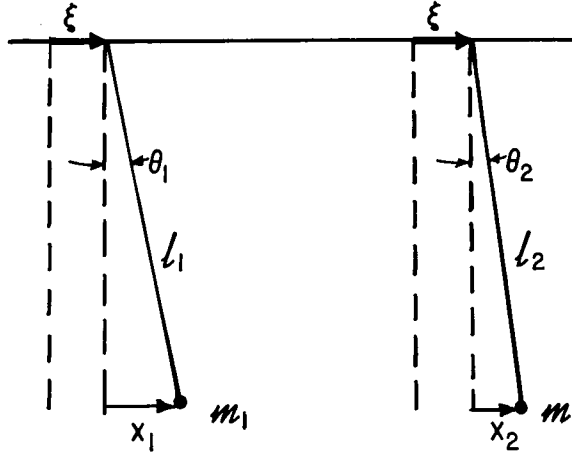


Fig. 3 — Common-moding arrangement without isolation

in vacuum, internal friction is presumably the only dissipative force, and since this must depend on displacement of the masses with respect to the vertical, only the x coordinates can be involved. Therefore, any damping coefficient associated with the ξ coordinate must be zero. If the pendulums are in air, friction from motion through the air arises from changes in both the x and ξ coordinates. Since this case might arise in a laboratory simulation of the procedure, it will be considered initially. Thus, for m_1 the equation of motion is

$$m_1(\ddot{x}_1 + \ddot{\xi}) = -(r_{x_1}\dot{x}_1 + r_{\xi}\dot{\xi}) - T_1\theta_1, \quad (25a)$$

and for m_2 it is

$$m_2(\ddot{x}_2 + \ddot{\xi}) = -(r_{x_2}\dot{x}_2 + r_{\xi}\dot{\xi}) - T_2\theta_2 + F_2. \quad (25b)$$

The subscripted r 's are damping coefficients. Employing the usual small-angle approximations yields $T_1 = m_1g$, $T_2 = m_2g$, $\theta_1 = x_1/l_1$, and $\theta_2 = x_2/l_2$. If these substitutions are made, and if $g/l_1 = \omega_1^2$ and $g/l_2 = \omega_2^2$, where the ω 's are the angular frequencies of the undamped pendulum oscillation, the equations of motion become

$$\ddot{x}_1 + \ddot{\xi} + \frac{r_{x_1}}{m_1}\dot{x}_1 + \frac{r_{\xi}}{m_1}\dot{\xi} + \omega_1^2x_1 = 0 \quad (26a)$$

and

$$\ddot{x}_2 + \ddot{\xi} + \frac{r_{x_2}}{m_2}\dot{x}_2 + \frac{r_{\xi}}{m_1}\dot{\xi} + \omega_2^2x_2 = F_2. \quad (26b)$$

If the pendulums are matched so that their masses, lengths, and air friction are identical (in vacuum, only their masses and not their shapes need be identical), the equation of motion for the relative coordinate $x_2 - x_1$, which results from subtracting the above equations, is

$$\frac{d^2}{dt^2} (x_2 - x_1) + \frac{r_x}{m} \frac{d}{dt} (x_2 - x_1) + \omega_0^2 (x_2 - x_1) = F_2. \quad (27)$$

When the pendulums are matched, motions of the upper support plane have no effect on the motion of the relative coordinate which now responds to the force on one pendulum bob as if it were in a noise-free environment. Thus, all the analysis following Eq. (1) applies.

Unfortunately, this state of mathematically perfect noise compensation cannot in practice be achieved due to mismatches of the resonance frequencies and decay times of the two pendulums. For a given degree of noise rejection, a particular accuracy of frequency and time-constant matching of the two pendulums will be required. This may be computed from Eqs. (26). If one assumes that the support plane specified by coordinate ξ undergoes the sinusoidal motion $\xi = C \exp(i\omega t)$, then the coordinates x_1 and x_2 will respond as $x_1 = A \exp(i\omega t)$ and $x_2 = B \exp(i\omega t)$, with complex amplitudes A and B determined by Eqs. (26). Substituting the assumed forms into Eq. (26) yields

$$A \left(\omega_1^2 - \omega^2 + \frac{2}{\tau_1} i\omega \right) = \left(-\frac{r_\xi}{m} i\omega + \omega^2 \right) C$$

and

$$B \left(\omega_2^2 - \omega^2 + \frac{2}{\tau_2} i\omega \right) = \left(-\frac{r_\xi}{m} i\omega + \omega^2 \right) C.$$

Since $(r_\xi/m)\omega$ is very small compared to ω^2 , it will be neglected. Thus for the complex relative displacement amplitude one has

$$B - A = \omega^2 C \left(\frac{1}{\omega_2^2 - \omega^2 + \frac{2}{\tau_2} i\omega} - \frac{1}{\omega_1^2 - \omega^2 + \frac{2}{\tau_1} i\omega} \right). \quad (28)$$

We now make the substitutions $\omega_2^2 = \omega_1^2 + \Delta$ and $1/\tau_2 = 1/\tau_1 + 1/\delta$, where Δ and $1/\delta$ are small. We further define $\omega_1^2 - \omega^2 + (2/\tau_1)i\omega \equiv Z$ and $\Delta + 2i\omega/\delta \equiv D$. With these definitions, Eq. (28) becomes

$$B - A = -\frac{\omega^2 CD/Z^2}{1 + D/Z}, \quad (29)$$

where $A = \omega^2 C/Z$. This amplitude is the noise amplitude that would be observed in pendulum 1 alone due to vibrational motion of its pivot at frequency ω_1 . (Under the

conditions of laboratory measurement mentioned previously, the magnitude of A was approximately $10 \mu\text{m}$.) Thus, the ratio $(B-A)/A$ specifies the degree of noise reduction brought about by the compensation scheme. The smaller this number is, the greater the chances of successful completion of the measurements. Initially it will be set equal to 10^{-4} .† Computationally, the reciprocal of this ratio is easier to manipulate than the ratio itself. Since it is complex, we set it equal to $10^4 \exp(i\theta)$. Thus,

$$\frac{-A}{B-A} = 1 + \frac{Z}{D} = 10^4 e^{i\theta}. \quad (30)$$

or, approximately

$$\frac{Z}{D} \approx 10^4 e^{i\theta}.$$

Further,

$$\left[\frac{Z}{D} \frac{Z^*}{D^*} \right]^{1/2} = \frac{[(\omega_1^2 - \omega^2)^2 + 4\omega^2/\tau_1^2]^{1/2}}{[\Delta^2 + 4\omega^2/\delta^2]^{1/2}} = 10^4. \quad (31a)$$

It is now convenient to assume that

$$4\omega^2/\delta^2 = \Delta^2. \quad (31b)$$

We consider two cases. In the first, we set the drive frequency equal to $\sqrt{2} \omega_1$, and in the second, equal to ω_1 . In case 1, the term in $1/\tau^2$ in the numerator is small compared to the term in ω_1^4 , and we find immediately from Eq. (31) that

$$\Delta = \frac{\omega_1^2}{\sqrt{2} 10^4}. \quad (32)$$

Since $\Delta = 2\omega_1 d\omega_1$ and $d\omega_1 = \omega_1 dT_1/T_1$, then $\Delta = 2\omega_1^2 dT_1/T_1$, and from Eq. (32),

$$\frac{dT_1}{T_1} = \frac{1}{2\sqrt{2} 10^4}. \quad (33)$$

This degree of precision is relatively high but probably achievable. (The means for achieving it will be discussed in later sections.) We now obtain the precision requirements for $1/\delta$. From Eqs. (31b) and (32), we have

†A noise amplitude of $10 \mu\text{m}$ in this case would be reduced to $10^{-3} \mu\text{m} = (10^{-3} \mu\text{m}/0.63 \mu\text{m})$ fringes = 1.6×10^{-3} fringes. From Eq. (21b), we find that a S/N ratio of 1 would occur after three cycles of driving the pendulum.

$$\frac{1/\delta}{1/\tau} = \frac{\tau\omega_1}{4 \times 10^4}.$$

τ will be assumed to be of the order of 10^3 or greater on the basis of the preliminary laboratory measurements, so we find the deviation $1/\delta$ in the line width $1/\tau$ of the two pendulums to be

$$\frac{1/\delta}{1/\tau} = \frac{\omega_1}{40} \quad (34)$$

or greater. Thus, the damping times need not be matched with the same precision as the center frequencies or periods. By suspending the pendulums identically, we will assume that the precision requirement of Eq. (34) can be met.

We now consider the second case, that in which the noise frequency is precisely tuned to the pendulum resonance at ω_1 . Again, for convenience, we assume that $4\omega^2/\delta^2 = \Delta^2$. Setting $\omega = \omega_1$ in Eq. (31a) leads immediately to

$$\frac{2\omega_1}{\tau_1\sqrt{2}\Delta} = 10^4.$$

Using the fact that $\Delta = 2\omega_1^2 dT_1/T_1$, we obtain

$$\frac{dT_1}{T_1} = \frac{1}{\sqrt{2}\omega_1 10^7} \quad (35)$$

for the necessary accuracy of frequency matching between the two pendulums. We see that on resonance, due to the amplification of the pivot motion by each pendulum, the compensation must be extremely precise, probably too precise for practical application. The corresponding requirement on $1/\tau_1$ can be found as before;

$$\frac{1}{\delta} = \frac{\Delta}{2\omega_1} = \omega_1 \frac{dT_1}{T_1} = \frac{1}{\sqrt{2} 10^7}.$$

Hence,

$$\frac{1/\delta}{1/\tau} = \frac{\tau}{\sqrt{2} 10^7} = \frac{1}{\sqrt{2} 10^4}. \quad (36)$$

The requirement on the line width is, as in the nonresonance case, much less severe than the tuning requirement. That this result is physically reasonable can be seen by inspection of Eqs. (26a) and (26b). The velocity terms are multiplied by constants r_x/m which are assumed to be of the order of 10^{-3} or smaller. These terms consequently affect the motion to a relatively small degree.

Common-Mode Method With Isolation

The failure of the common moding scheme, shown in Fig. 3, to effectively shield the system from noise frequencies at ω_1 may be ameliorated by the arrangement in Fig. 4. With small-angle approximations as before, the equation of motion for the ξ coordinate of the intermediate platform is given by

$$m\ddot{\xi} = mg \frac{x_1}{L_1} + mg \frac{x_2}{L_2} - (2m_1 + m) \frac{g}{l} (\xi - \xi')$$

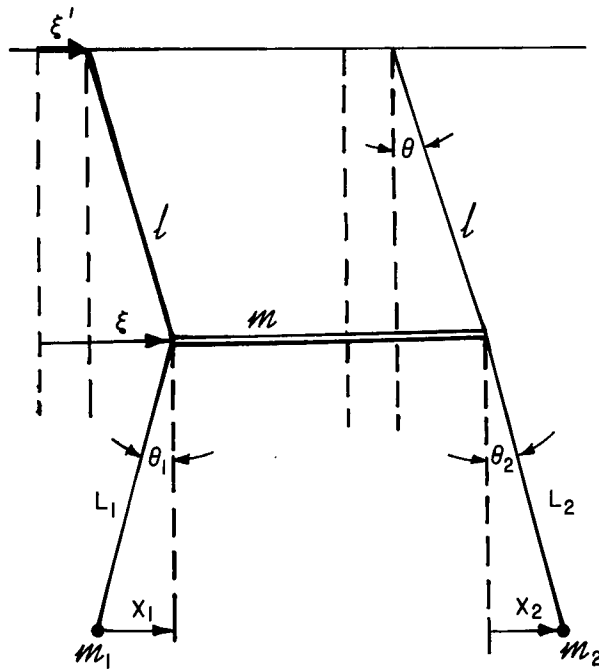


Fig. 4 — Common-moding arrangement with isolation

The following definitions allow a more compact notation:

$$\frac{g}{l} = \omega_0^2, \quad \frac{g}{L_1} = \omega_1^2, \quad \frac{g}{L_2} = \omega_2^2$$

$$M = 2m_1 + m, \quad \frac{m_1}{M} = \mu, \quad \text{and } \frac{m}{M} = \mu_0.$$

After these substitutions have been made, the equation is transformed to read

$$\mu_0 \ddot{\xi} - \mu \omega_1^2 x_1 - \mu \omega_2^2 x_2 + \omega_0^2 \xi = \omega_0^2 \xi', \quad (37)$$

where coordinate ξ' is in effect the driving force. The equations for x_1 and x_2 are the same as Eqs. (26a) and (26b), and if the two lower pendulums are exactly matched, may be subtracted as before to yield Eq. (27). We are interested in the vibration isolation capabilities of the system in the face of a slight mismatch of the frequencies of the lower pendulums, ω_1 and ω_2 . Making the substitutions $x_1 = A \exp(i\omega t)$, $x_2 = B \exp(i\omega t)$, $\xi = C \exp(i\omega t)$ and $\xi^1 = \xi_0^1 \exp(i\omega t)$, one obtains the following equations in the coefficients:

$$\begin{aligned} -\mu \omega_1^2 A & & -\mu \omega_2^2 B & & + (\omega_0^2 - \mu_0 \omega^2) C & = \omega_0^2 \xi_0^1, \\ \left(-\omega^2 + \omega_1^2 + \frac{i\omega 2}{\tau}\right) A & & & & + \left(-\omega^2 + \frac{i\omega 2}{\tau}\right) C & = 0, \\ & & \left(-\omega^2 + \frac{i\omega 2}{\tau} + \omega_2^2\right) B & & + \left(-\omega^2 + \frac{i\omega 2}{\tau}\right) C & = 0. \end{aligned} \quad (38a)$$

For simplicity, r_x/m_1 has been set equal to $r_\xi/m_1 = 2/\tau$. It is useful to contract the notation by using the definitions

$$z_1 = -\omega^2 + \omega_1^2 + i\omega 2/\tau, \quad z_2 = -\omega^2 + \omega_2^2 + i\omega 2/\tau,$$

and

$$z = \omega_0^2 - \mu_0 \omega^2. \quad (38b)$$

Then we find that

$$A = \frac{1}{E} \omega_0^2 \xi_0^1 [-z_2(-\omega^2 + i\omega 2/\tau)], \quad (39a)$$

and

$$B = -\frac{\omega_0^2 \xi'_0 z_1}{E} (-\omega^2 + i\omega 2/\tau), \quad (39b)$$

where E is the determinant of the coefficients, given by

$$E = \mu\omega_1^2(-\omega^2 + i\omega 2/\tau)z_2 + z_1[\mu\omega_2^2(-\omega^2 + i\omega 2/\tau) + zz_2]. \quad (39c)$$

It is useful to examine the behavior of A and B without damping ($\tau = \infty$) for ω_1 equal to ω_2 . In this case,

$$A = B = \frac{\omega_0^2 \xi'_0 \omega^2}{-2\mu\omega_1^2 \omega^2 + (\omega_0^2 - \mu_0 \omega^2)(-\omega^2 + \omega_1^2)}.$$

Further, when the noise oscillation occurs at $\omega = \omega_1$, which is a resonance frequency of the system,

$$A = B = -\frac{\omega_0^2 \xi'_0}{2\mu\omega_1^2}.$$

The fact that the motion is finite indicates that the resonance mode cannot be driven by the force ξ' . This is in agreement with intuition, since in the normal mode at frequency ω_1 the two lower pendulums must move in exactly opposite directions, with the upper platform stationary. But the only way that the pendulums can experience forces due to the oscillation of ξ' is through the motion of the upper platform. Hence, this mode cannot be driven by coordinate ξ . We therefore expect the system shown in Fig. 4 to be considerably more immune to vibrational noise at the signal frequency ω_1 than the previous system. To calculate the precise degree of noise rejection, we return to Eqs. (39) and form the difference $B - A$ as was done previously. This difference coordinate should be compared with the response of a nonisolated pendulum with the same resonance frequency. This response, denoted by A_0 , is

$$A_0 = \frac{\omega^2 \xi'_0}{\omega_1^2 - \omega^2 + 2i\omega/\tau}.$$

Using the expressions of Eq. (39) yields $(B - A)/A_0$, the noise rejection ratio;

$$\frac{B - A}{A_0} = \frac{\omega_0^2}{\omega^2} \frac{z_1}{E} (-\omega^2 + i\omega 2/\tau)(\omega_2^2 - \omega_1^2). \quad (40)$$

For convenience, ω_0^2 is taken to be $2\omega_1^2$, which implies that the length of the upper pendulum is half that of the lower. It is now necessary to evaluate Eq. (40) for different values of

$(\omega_2 - \omega_1)/\omega_1$, with ω set equal to each of the roots of E in turn in order to examine the noise rejection of the system at each of its resonance frequencies. The resonance frequencies are found from Eq. (39c) with τ set equal to infinity. Since E is a cubic in ω^2 , the algebra involved in explicitly writing Eq. (40) with $\omega = \omega_j(\omega_1, \omega_2)$, $j = 1, 2, 3$, where $\omega_j(\omega_1, \omega_2)$ is a root of E , is prohibitively difficult.

Therefore, it was decided to obtain the results numerically. A program was written which did the following. For given values of τ, μ, μ_0 , and ω_1 , an initial value of ω_2 was computed which differed from ω_1 by one part in 10^4 . Roots of E with $\tau = \infty$ were then computed, and with ω set equal to each root in turn, $|(B - A)/A_0|$ was computed and compared to 10^{-4} . If the rejection ratio was larger than 10^{-4} for any of the roots, a new value of ω_2 was computed whose deviation from ω_1 divided by ω_1 was half the previous value. The computations of the rejection ratio, for this better-matching pair of frequencies, were carried out and the process was repeated until the rejection ratio was smaller than 10^{-4} for each root of E for a given pair of frequencies ω_1 and ω_2 . The important results are shown in Table 1. The upper section of the table labeled *satellite* corresponds to a value of 10 for the satellite-to-upper-platform mass ratio. Values of μ and μ_0 can be computed from the mass ratio. The periods and corresponding frequencies are computed from Δ , with $\omega_1 = \omega_2 = 2\pi$ and $\tau = \infty$. The lower half of the table labeled *simulation* was computed using a satellite-to-upper-platform mass ratio of 1/20. The terms *satellite* and *simulation* have been associated with these mass ratios, since they are the ratios which have resulted from initial mechanical design considerations applied to the two cases.

Table 1 — Noise-Rejection Ratios for Various Degrees of Frequency Mismatch

$T(1)$	$\nu(1)$	$\left \frac{B-A}{A} \right _1$	$T(2)$	$\nu(2)$	$\left \frac{B-A}{A} \right _2$	$T(3)$	$\nu(3)$	$\left \frac{B-A}{A} \right _3$	$(\omega_2 - \omega_1)/\omega_1$
Satellite $\mu_0 = 0.0476190476$									
1.0	1.0	$< 10^{-4}$	1.2	.833	$< 10^{-4}$	0.12	8.33	$< 10^{-4}$	$< \frac{1}{6 \times 10^7}$
		10^{-4}			10^{-1}			2.5	$\frac{1}{4 \times 10^4}$
		4×10^{-4}			0.5			10	$\frac{1}{10^4}$
Simulation $\mu_0 = 0.9090909091$									
1.0	1.0	$< 10^{-4}$	1.04	.961	$< 10^{-4}$	0.65	1.53	$< 10^{-4}$	$< \frac{1}{6 \times 10^7}$
		10^{-4}			0.03			0.4	$\frac{1}{3 \times 10^5}$
		10^{-3}			0.26			3.1	$\frac{1}{4 \times 10^4}$
		4.6×10^{-3}			1.0			12.3	$\frac{1}{10^4}$

It is immediately clear from looking at the table that it is impractical to demand a rejection ratio smaller than 10^{-4} for each of the three resonance frequencies, since the frequency match of ω_2 and ω_1 would then have to be closer than 10^{-7} . A more reasonable strategy would seem to be to demand a high degree of rejection for noise at the signal frequency $\nu(1)$, and then to use electronic notch filters to eliminate noise at the other two resonance frequencies. The table shows that in this case the requirements on $(\omega_2 - \omega_1)/\omega_1$ are relaxed to the point of tractability since the periods of repetitive waveforms can be measured to $1/10^5$, and waveforms for timing purposes can be synthesized to the same accuracy [4]. Electronic notch filters can be constructed to reject the output resulting from noise at the resonance frequencies corresponding to roots 2 and 3 in the satellite case since these are reasonably well separated, but this is considerably more difficult in the simulation case. It might prove necessary to increase the mass of the simulated satellite in this case in order to increase the separation of the resonance frequencies. A mass ratio $m_1/m = 0.5$ results in a separation of 13% for the two closest frequencies, which is probably great enough to allow the design of a notch filter to reduce response at the nonsignal frequency by a factor of 10^{-4} [4] while not substantially affecting that at the signal frequency. It should be noted that for the present mechanical arrangement, there is a maximum attainable separation for the two closest roots, given the possible range of variation of μ_0 . This can be found from the expression for E in Eq. (39c) by setting ω_2 equal to ω_1 . For this condition, and with τ set equal to infinity, one obtains

$$E_{\omega_2=\omega_1} = (-x + \omega_1^2)(\mu_0 x^2 - 3\omega_1^2 x + 2\omega_1^4), \quad (41a)$$

where $x \equiv \omega^2$. The roots of this expression are easily found to be

$$x = \omega_1^2, \quad \text{and} \quad x = \omega_1^2 \left[\frac{3 \pm (9 - 8\mu_0)^{1/2}}{2\mu_0} \right]. \quad (41b)$$

The root closest to that corresponding to the signal frequency ω_1 results when the minus sign is taken. For $\mu_0 = 1$, this root is $x = \omega_1^2$, while in the limit $\mu_0 \rightarrow 0$, $x = 2/3\omega_1^2$ or $\sqrt{x} = 0.816\omega_1$. Thus, the largest frequency separation achievable between ω_1 and its nearest neighbor is about 18%.

Additional Frequency-Matching Criterion

There is still another error component similar in nature to that leading to Eq. (12). It is the change in the overall response of the relative coordinate of the two pendulums due to a slight mismatch of their frequencies, even though the driving force is exactly on the resonance of one of the pair. We will compute the error for the infinite time case and assume that the precision required in the finite time case is less, as in the situation existing between Eqs. (12) and (13). The case in question is readily treated by a modification of Eq. (38a). These equations describe the motion of the triple pendulum due to sinusoidal oscillation of the ceiling of amplitude ξ'_0 .

In the present case, ξ'_0 is set equal to zero, and the amplitude f of a sinusoidal signal is inserted as the right-hand side of the third equation of the set. By defining $z_3 = -\omega^2 + i\omega 2/\tau$ in addition to the previous definitions for z_1 , z_2 , and z , we obtain the compact equations

$$\begin{aligned} -\mu\omega_1^2 A - \mu\omega_2^2 B + zC &= 0, \\ z_1 A + z_3 C &= 0, \\ z_2 B + z_3 C &= f. \end{aligned} \tag{42a}$$

Using determinants, one immediately obtains

$$A = -\frac{f\mu\omega_2^2 z_3}{E} \tag{42b}$$

and

$$B = \frac{f}{E} (\mu\omega_1^2 z_3 + z z_1),$$

where

$$E = \mu\omega_1^2 z_3 z_2 + z_1 (\mu\omega_2^2 z_3 + z z_2). \tag{42c}$$

The measured response, for $\omega_2 \neq \omega_1$, is $B - A$, or

$$B - A = \frac{f}{E} [\mu z_3 (\omega_1^2 + \omega_2^2) + z z_1]. \tag{43a}$$

The formula used for computation in ignorance of the frequency mismatch would be that obtained by setting $\omega_2 = \omega_1$ in Eq. (43a), or just

$$(B - A)_{2 \rightarrow 1} = \frac{f}{z_1}. \tag{43b}$$

The subject of the present inquiry is the ratio of Eq. (43a) to Eq. (43b) when the driving frequency is assumed to be at ω_1 . Specifically, the ratio is

$$\frac{B - A}{(B - A)_{2 \rightarrow 1}} = \frac{z_1}{E} \left\{ \mu z_3 (\omega_1^2 + \omega_2^2) + z z_1 \right\}. \tag{44}$$

Replacing ω_2^2 by $\omega_1^2 + \Delta$, we may write

$$E = z_1(2\mu\omega_1^2 z_3 + z z_1) \left[1 - \Delta \frac{(\mu\omega_1^2 z_3 + \mu z_1 z_3 + z_1 z)}{z_1(2\mu\omega_1^2 z_3 + z z_1)} \right]. \quad (45a)$$

Similarly, the numerator of Eq. (44) may be written in the form

$$z_1(2\mu z_3 \omega_1^2 + z z_1) \left[1 + \frac{\Delta \mu z_3}{2\mu z_3 \omega_1^2 + z z_1} \right]. \quad (45b)$$

It is now necessary to evaluate z , z_1 , and z_3 , at $\omega = \omega_1$. We have $z_3 = -\omega_1^2 + i\omega_1 2/\tau \approx -\omega_1^2$ since $\tau \approx 10^3$ s, $z = \omega_1^2(2 - \mu_0)$, and $z_1 = i\omega_1 2/\tau$. After expression (45b) is divided by Eq. (45a) and the values for z , z_1 , and z_2 are inserted, Eq. (44) becomes

$$\frac{B - A}{(B - A)_{2 \rightarrow 1}} = \frac{1 + \frac{-\mu\omega_1^2 \Delta}{-2\mu\omega_1^4 + 2\omega_1^3 i(2 - \mu_0)/\tau}}{1 + \frac{\Delta(-\mu\omega_1^4 - 2\mu i\omega_1^3/\tau + 2i\omega_1^3(2 - \mu_0)/\tau)}{\frac{2i\omega_1}{\tau} (-2\mu\omega_1^4 + 2i\omega_1^3(2 - \mu_0)/\tau)}}.$$

Evidently, terms in $1/\tau$ in the sums may be dropped so that the result simplifies to

$$\frac{B - A}{(B - A)_{2 \rightarrow 1}} = (1 + \Delta/2\omega_1^2)(1 + \Delta\tau/2i\omega_1^2)^{-1}.$$

We now assume that $\Delta < 1/\tau$ so that the second parenthesis can be expanded by using the binomial expansion. It easily follows that

$$\left| \frac{B - A}{(B - A)_{2 \rightarrow 1}} \right| \approx 1 + \frac{\Delta^2 \tau^2}{8\omega_1^4}. \quad (45c)$$

For a 1% error resulting from the incorrect use of the expression for $(B - A)_{2 \rightarrow 1}$,

$$\frac{\Delta\tau}{2\sqrt{2}\omega_1^2} = 10^{-1}.$$

Since $\Delta = 2\omega_1 d\omega_1$, and $dT/T = d\omega_1/\omega_1$,

$$\frac{dT}{T} \approx \frac{1}{7\tau}. \quad (46)$$

Time-Saving Method

An additional technique may be employed if the noise in a particular environment turns out to be much larger than that considered here after use of the noise-rejection scheme but is still small compared to the maximum signal deflection obtainable. In this case the pendulum would have to be driven through many oscillations before a really useful S/N ratio could be achieved. It would appear that measurement time could be saved as follows. The noise motion of the pendulum is monitored and the phase precisely determined. (For times short compared to the damping time, the motion should appear sinusoidal.) Relatively precise knowledge of the phase is used to fix the instant of initiation of the first signal-driving pulse so that the response to it is $\pi/2$ rad out of phase with the noise oscillation. The output signal of the pendulum motion transducer is then fed into a phase-sensitive detector which greatly reduces the noise output after a very few cycles. The outcome of this procedure should be to achieve a relatively high S/N ratio using much shorter observation times than would otherwise be necessary.

An example will make this clearer. Suppose that in the case of the simulation experiment, for which the maximum amplitude response was calculated to be $2.42 \mu\text{m}$, the noise after rejection was $2.4 \times 10^{-2} \mu\text{m}$, so that the intrinsic S/N ratio was 100/1. Unfortunately, the amplitude of the response of the pendulum, according to Eq. (21b), would be 6.6×10^{-4} fringes per signal pulse, so that to attain an amplitude of $0.024 \mu\text{m}/0.63 \mu\text{m} = 0.04$ fringes, or a S/N ratio of 1, would take about 60 pulses. But, if the signal were phased to be in quadrature with the noise oscillation at $t = 0$, the noise would no longer have the advantage of having been on for a long time compared with the signal and would be quickly integrated to zero.†

Mechanical Requirements for Frequency Matching

Signal-to-noise requirements for this problem dictate that the frequencies of the two pendulums be matched as precisely as possible. Based on considerations given in previous sections and the data shown in Table 1, we will take as our design goal a frequency match of $1/10^5$ for the simulation case and $1/10^4$ for the satellite case. A number of general mechanical tolerance relations, which were derived in the third section, as well as certain new criteria, take on concrete numerical values in the context of these choices for the noise-rejection ratio.

†This technique depends on the noise having a sinusoidal rather than an impulsive character. It is also assumed that the internal noise of the motion transducer is much less than the residual noise oscillation of the pendulum system. The latter condition is easy to fulfill.

A primary consideration is the precision of frequency definition of the pendulum of finite amplitude without damping. This is given by Eq. (17). The worst case is the frequency measurement of the simulation experiment. Appropriate to this example are an initial pendulum displacement of 0.5 mm and a pendulum length of 25 cm. The corresponding angular displacement θ_0 is 2×10^{-3} rad. Since $k = \theta_0/2$, $k = 10^{-3}$ rad, and $k^2 = 10^{-6}$ rad², the variation of the period of the pendulum is $1/4 \times 10^6$, which is 40 times smaller than necessary even for this very large displacement.

The next consideration is whether the finite line width of a pendulum with dissipation is consistent with the design goal. This limitation to the precision of measurement is given by Eq. (16). In this equation, ϵ is the fraction of the peak amplitude necessary to trigger the clock used to measure the period of the waveform, T_1 is the period of the pendulum, and τ is its damping time. Again we consider the simulation to be the worst case. If $\epsilon = 1/20$, $\tau = 10^3$ sec, and $T_1 = 1$ sec, then the error in measurement is approximately $1/10^5$.

The most basic requirement, the stability of the frequency of the oscillator and its resulting measurability, seems to be met. Before the allowed precision can be realized, however, the length of the pendulum must be precisely adjustable. Since $T = 2\pi(l/g)^{1/2}$, it follows that $dT/T = + 1/2dl/l$. For $dT/T = 1/10^5$, we have $dl/l = 1/5 \times 10^4$. In the simulation case, $l = 25 \times 10^3 \mu\text{m}$, and $dl = 0.5 \mu\text{m}$. This is well within the range of differential screw micrometers. In the case of the satellite, dl is much larger, although the mass to be supported in this case is also much larger.

The specification of dl/l necessarily implies a requirement on the temperature stability of the system. This is readily determined from the standard equation for the differential change in length in terms of the temperature coefficient of expansion α and the temperature change dT or, $dL = L\alpha dT$. For high-carbon steel wire, α is commonly of the order of $10^{-5}(k^{-1})$. Thus, $dL/L = 10^{-5}dT$, so that the allowed temperature variation is about 1 kelvin.

The remaining effect which could alter the length of the pendulum is creep. For carbon steel wire, work hardening after the initial strain causes the creep to approach zero [5]. Since whatever creep there is would tend to be the same for both pendulums, it would appear that this problem should be manageable so far as the length match required for noise rejection is concerned.

The error in using the resonance equation due to imprecise location of the frequency of the driving signal is 1% for the accuracy criterion of Eq. (12). For $\tau = 10^3$ sec and $\omega_1 = 2\pi$ Hz, we obtain $dT/T \approx 1/6 \times 10^4$. However, this requirement is more stringent than is necessary to satisfy Eq. (14). If the frequencies are matched initially with sufficient precision to realize a large noise-rejection ratio, their subsequent drift, if the same for both, as would be indicated by the continued rejection of noise, would be unlikely to be large enough to cause errors due to the use of Eq. (13) with ΔT set equal to zero. Last, we consider the frequency-match error criterion for the use of Eq. (43b). This is given by Eq. (46). For $\tau = 10^{-3}$ sec, we have $dT/T \approx 1/10^4$, which is not more stringent than any of our other requirements.

OPTICAL MONITORING SYSTEM

Interferometer

The method of measuring the difference coordinate $x_2 - x_1$ of the two pendulums will now be described. An interferometer is the natural choice of instrument for this kind of measurement, and an arrangement which can satisfy the somewhat novel demands of the observation at hand is shown in Fig. 5. The two-beam interferometer has been realized with components having a large number of invariances to possible motions arising due to vibrational noise. The initial beam, which enters from the lower right, is split by a Jamin plate into two parallel, horizontal beams one above the other. These beams are incident upon two roof-edge reflectors. The upper reflector is to be imagined as being attached to a pendulum, the lower one as attached to the ground. After reflection, the two beams are incident on a second set of roof-edge reflectors which send them to a second Jamin plate where they recombine and interfere on the surface of a pin-diode detector. The second pair of roof-edge reflectors is arranged identically to the first, with the upper member of the pair attached to the second of the two pendulums. The lateral displacement of the reflected beams requires that the reflectors be located off center on the pendulum platforms. The resultant shift of the center of mass of the pendulums may be compensated for by appropriate loading. With this arrangement, it may be seen that there is no change in the optical path of the upper beam when the two upper corner reflectors move in the same direction. However, when they move in opposite directions, the optical path change is twice their difference coordinate. In use, the upper roof-edge reflectors would be adjusted to reasonable alignment and the fine alignment of the system would be carried out on the fixed components below.

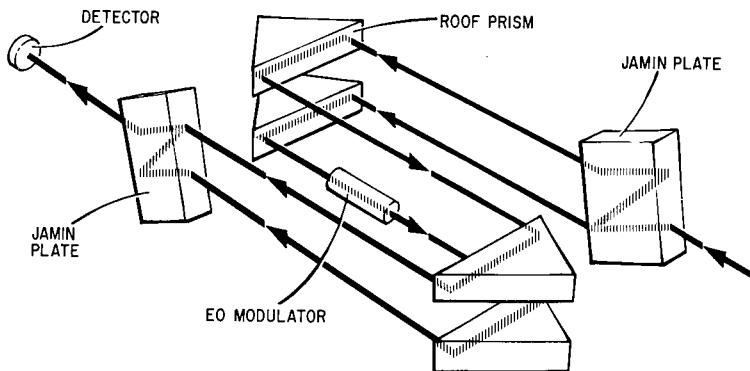


Fig. 5 — Interferometer for measuring changes in the difference coordinate

One important optical component remains to be mentioned. This is an electro-optic modulator to be placed in the lower beam. Its purpose is to furnish test signals for precise adjustment of the optical path of the lower beam and to furnish calibration signals during the measurement procedure. The path difference between the two beams should be such that the small oscillations in detected power that constitute the signal occur in the middle of the ramp of the sinusoidal response of the interferometer. This condition can be realized by driving the modulator so that the optical path oscillation is slightly greater than $\lambda/4$ in each direction. One of the lower corner reflectors is then translated toward or away from the other until the signal from the detector, as seen on an oscilloscope, appears as in Fig. 6 with a notch symmetrically placed at either end of the ramp. When the oscillating voltage applied to the modulator is decreased to a small amplitude, the waveform applied (a triangle is very useful for this purpose) should be accurately reproduced in the output of the interferometer.

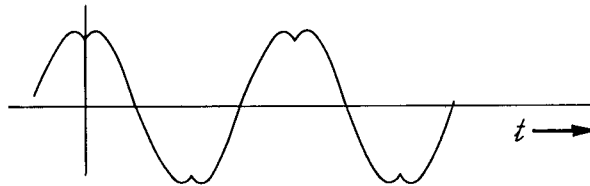


Fig. 6 — Detector output for optical path variation greater than $\lambda/4$ with interferometer in adjustment

Once the path change corresponding to a given voltage amplitude is known, any other waveform amplitude may be measured. It is sometimes convenient to employ a calibration signal of small amplitude and high frequency so that many cycles occur in one period of the signal. Then the appearance of the calibration signal gives continuous information on the state of adjustment of the system during the course of observations. If the amplitude of the calibration signal is sufficiently small, it only marginally affects measurement of the signal.

Invariance Properties of Roof-Edge Reflectors

The invariance properties of the roof edge reflectors must now be treated in detail since they are very important in the rejection of possible spurious noise oscillations of the pendulum platforms which could otherwise affect the measurements. We are not speaking here of the modes of motion along the direction of propagation of the light beam, which have already been discussed. These are necessarily detected by the interferometer and are distinguishable from the signal in the detector output only by their frequency. We are considering small oscillations and rotations outside of the plane of expected linear motion, which might occur because of a lack of perfect operation of the constraints described on page 17.

First we consider the effect of rotations of the roof reflector on the phase of the reflected light beam. See Fig. 7. Initially, a hollow roof edge composed of two intersecting mirror surfaces is studied. The effect of the glass in a porro-prism roof-edge reflector will be seen later.

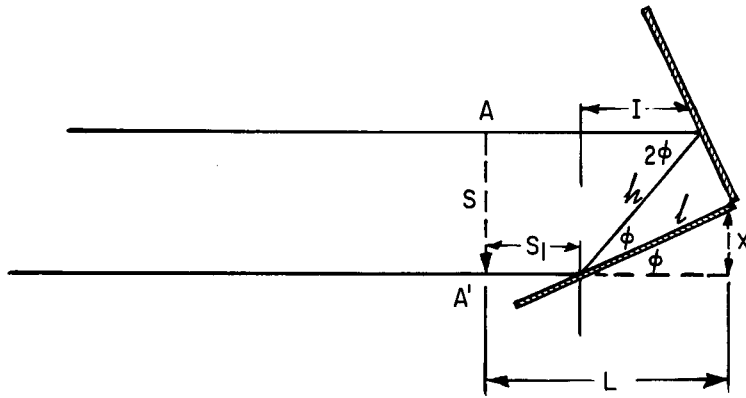


Fig. 7 — Diagram for calculation of effect of rotational orientation of roof edge on optical path

The path P from an arbitrary plane AA' to the roof edge and back is computed. Inspection of the figure shows that this is

$$P = 2S_1 + h + I,$$

where

$$S_1 = L - x \cot \phi$$

and

$$h = \frac{\ell}{\cos \phi} = \frac{x}{\sin \phi \cos \phi}.$$

Further,

$$h + I = h(1 + \cos 2\phi) = 2x \cot \phi.$$

Substituting S_1 and $h + I$ into the expression for P , we find that

$$P = 2L. \tag{47}$$

This result means that the optical path is insensitive to both rotations and lateral translations of the roof edge as long as the distance from the vertex to the plane does not change. Thus, the effects of rotation of the platforms may be minimized by placing the vertices of the reflectors over the centers of mass of the pendulums.

A change in the separation S of the ingoing and outgoing beams would result in a relative shear of the interferometer beams upon recombination. The effect on shear of reflector motion in a horizontal plain is easily computed. From the geometry of Fig. 7, we have

$$S = h \sin 2\phi = \frac{x \sin 2\phi}{\sin \phi \cos \phi} = 2x.$$

The only differential relationship possible is

$$dS = 2dx. \quad (48)$$

Hence, rotation of the reflector does not effect shear, but lateral translation does. The contribution of small variations in shear to noise in the detector output may be computed as follows. The light wave that has traversed the upper path (see Fig. 5) is represented by $U_1 \exp [(2\pi i L_1)/\lambda]$ in the plane of the detector surface after the second Jamin plate. The beam that has traversed the lower path is represented by $U_2 \exp [(2\pi i L_2)/\lambda]$ in the same plane. The sum of the two fields is thus

$$U_1 e^{\frac{2\pi i L_1}{\lambda}} + U_2 e^{\frac{2\pi i L_2}{\lambda}},$$

and the irradiance is

$$I = U_1^2 + U_2^2 + 2U_1 U_2 \cos \frac{2\pi(L_1 - L_2)}{\lambda}. \quad (49a)$$

Note that the transverse dependence of the amplitudes U_1 and U_2 is not explicitly indicated in the notation. Equation (49a) holds, however, whether U_1 or U_2 are off or on at any given point in space. We will assume that the shear is small and that the detector is large enough to accept all the light in both beams. The total power P incident on the detector is the integral of I over its surface, or

$$P = \int_A I dx dy = \int_A \left[U_1^2 + U_2^2 + 2U_1 U_2 \cos \frac{2\pi(L_1 - L_2)}{\lambda} \right] dx dy. \quad (49b)$$

Since we are interested chiefly in the order of magnitude of the effect, it will be assumed that the beams are of rectangular cross section and of uniform, equal amplitude. For beams of y dimension b , and x dimension a , Eq. (49) immediately becomes

$$P = 2baU^2 \left[1 + \left(1 - \frac{\sigma}{a} \right) \cos \frac{2\pi(L_1 - L_2)}{\lambda} \right], \quad (49c)$$

where the shear is taken to be of magnitude σ and occurs in the x direction only. It is clear from Eq. (49c) that the interferometer is insensitive to small variation of $L_1 - L_2$ for $L_1 - L_2$ equal to zero. However, if the path difference is increased by $\lambda/4$, then for small variations ΔS in the path, the corresponding signal component of the output is

$$P_S = 2U^2 ab 2\pi \frac{\Delta L}{\lambda},$$

and the noise component due to shear variation is

$$P_N = 2U^2 ab 2\pi \frac{\Delta L}{\lambda} \left(\frac{\sigma}{a}\right).$$

The S/N ratio is thus given by

$$\frac{P_S}{P_N} = \frac{1}{\sigma/a}. \quad (50)$$

Thus, for a shear variation of 2% of the diameter of the beam, the S/N ratio is 50, which is satisfactory for present purposes. If a is 3 mm, then σ turns out to be 60 μm . It would appear that constraints on the pendulum motion could easily restrict lateral displacement to a value less than this since the amplitude of the completely unconstrained pendulum motion in the laboratory was less than this.

If the roof reflector consists of a right-angle prism, several other effects must be considered. Assume first that the prism is mathematically perfect, but that the light beam is not normally incident on the first surface. The situation is shown in Fig. 8. Inspection of the geometry of the figure shows that traversal through the prism is equivalent to propagation through a slab with parallel faces. Thus, while for a hollow roof edge, rotation about the vertex angle causes neither path change nor shear; for a prism roof edge, rotation causes both path length change and shear. Both, however, are second-order effects in the angle of incidence and may be made vanishingly small by precise alignment.

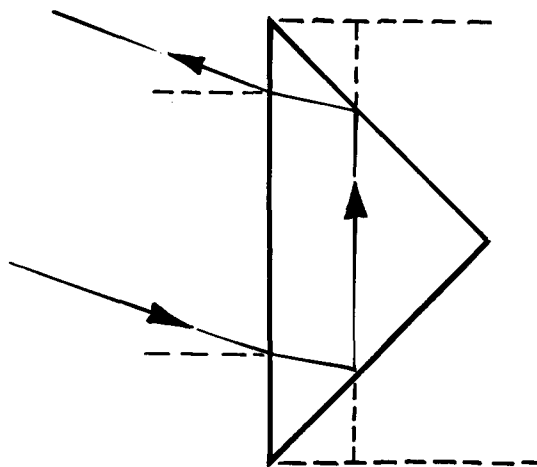


Fig. 8 — Diagram to determine effect of other than normal incidence of beam on roof-edge prism

The next question which must be answered for the prism reflector is the effect of the prism's not being isosceles. This may be investigated with the aid of Fig. 9. It follows easily from the geometry that angle $A = 2\theta_1$ and that therefore lines FF' and GG' are parallel, again implying that the prism looks like a glass plate to the incident light beam. Therefore the prism does not have to be accurately isosceles.

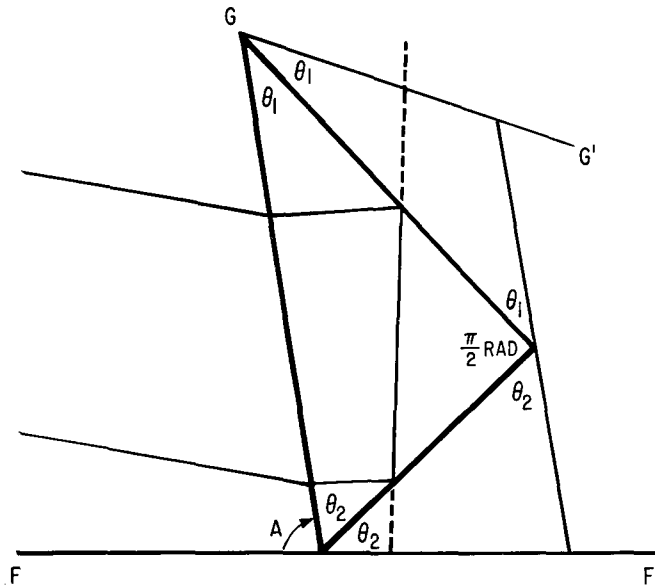


Fig. 9 — Diagram to determine effect of $\pi/2$ rad prism which is not isosceles

Another possible error is that the front face of the prism leans with respect to the apex angle. For purpose of calculation, assume that the beam is angled slightly with respect to the front surface of the prism so that, inside, it travels perpendicularly with respect to the vertex line. This situation is diagrammed in Fig. 10. It is of interest because the oscillation of the pendulums results in a small vertical translation that causes the wedge shown to oscillate vertically in the beam. If the horizontal amplitude is $50 \mu\text{m}$, then from the sagitta formula, the corresponding vertical amplitude for a pendulum 25 cm long is $5 \times 10^{-3} \mu\text{m}$. The path difference, in terms of fringes for double traversal of a wedge of angle θ , is

$$\frac{\delta}{\lambda} = \frac{2\theta(n-1)dx}{\lambda} \quad (51)$$

Restricting the maximum path error to $10^{-3}\lambda$ at $0.6328 \mu\text{m}$ and setting $dx = 5 \times 10^{-3} \mu\text{m}$, we have $\theta = 0.12 \text{ rad}$. This error is much larger than what would occur in a typical, well-made prism.

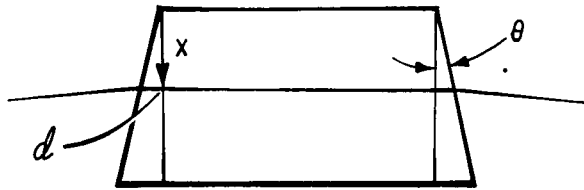


Fig. 10 — Diagram to determine effect of leaning of front face of prism with respect to apex angle

The final prism error which must be treated is an error ϵ in the apex angle. Figure 11 diagrams this situation. The effect on the beam is the same as it would be in traversing a glass plate with wedge angle 2ϵ . The error in waves is given by Eq. (51). For a $30\text{-}\mu\text{m}$ lateral displacement and a path error of 10^{-3} fringes, ϵ would be 2×10^{-5} rad. The fringe spacing in the output fringes due to this cause alone would be 15 mm. However, since there are four prisms involved, the fringe spacing would be about 1/4 of this value, or roughly equal to the diameter of a typical beam. If it were desired to relax the accuracy requirements on the apex angle on the grounds that $30\ \mu\text{m}$ of compensation of lateral motion against constraints was excessive, then an adjustable wedge (two matched wedges) could be used in the lower beam path to adjust the fringe spacing so that it still remained sufficiently large compared with the beam diameter.

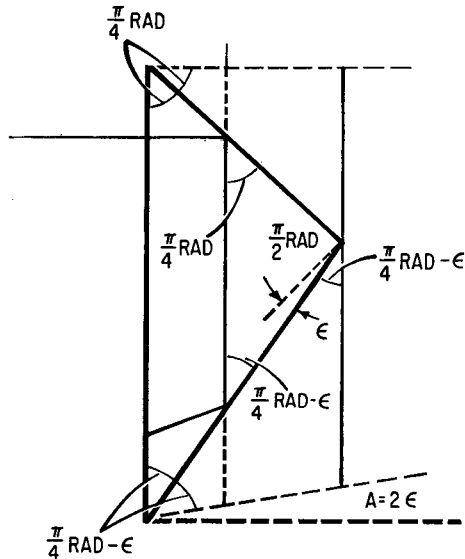


Fig. 11 — Diagram to determine effect of error in apex angle

Pendulum Frequency-Tuning Monitor

The interferometer used to measure the response of the relative coordinate of the two pendulums to the signal is not convenient for measuring the frequencies of the pendulums during the frequency-matching adjustments. The interferometer is suitable for measuring displacements that are small compared to the wavelength of light. But we have estimated in previous sections that the ambient noise will probably not be reduced to that level unless the frequencies are already matched. Before this condition obtains, small oscillation amplitudes will not occur. The interferometer response to large amplitudes of motion will consist of many cycles of sinusoidal oscillation. The period of such a waveform would be harder to measure than one linearly related to the pendulum displacement. A device is required for which the basic unit of measurement is considerably larger than a wavelength of light and larger than the amplitude to be measured. The moire fringes of a pair of Ronchi rulings arranged as in Fig. 12 nicely satisfy this condition. The gratings are placed on the pendulum tables so that the rulings are vertical. In this orientation they are maximally sensitive to the relative horizontal motion of the platforms, given the orientation of the two external mirrors and the imaging lens set for unit magnification. The spacing of the rulings and the amplitude of oscillation could be so chosen that the light transmission of the pair of rulings was linear in the pendulum displacement after proper adjustment. In this case the output of the detector system would be a sinusoidal signal, and the period of the sinusoid could be measured with an electronic frequency counter. Since the optomechanical system is symmetrical, repeated measurements could be made, alternating between the two pendulums without readjusting the optical system.

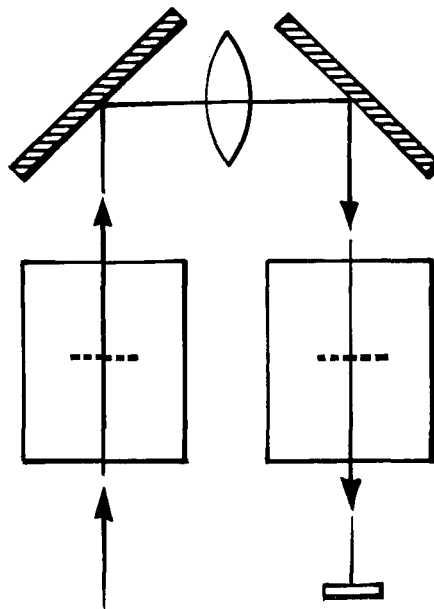


Fig. 12 — Pendulum tuning monitor

RADIOMETER FORCE

Historically, efforts to measure the pressure due to light were complicated by the radiometer effect. The radiometer effect refers to the increase in pressure exerted on a heated surface by a gas, above the pressure exerted when the surface is at the same temperature as the gas itself. It arises because the gas molecules that collide with the surface are heated in the process and leave the surface with greater momentum than they had before the encounter. This explanation holds in the case of very low pressure where the mean free path is large compared to the object of which the surface in question is a part, and compared to the dimensions of the container of the object. In this case the maximum pressure increase (coefficient of accommodation equals 1) is given by [6]

$$\Delta p = \frac{p}{2} \left[\left(1 + \frac{\Delta T}{T} \right)^{1/2} - 1 \right], \quad (52a)$$

which reduces, when $\Delta T/T$ is small, to

$$\Delta p \approx \frac{p}{4} \frac{\Delta T}{T}. \quad (52b)$$

It is of interest to calculate this pressure for the case of a satellite in an environmental test chamber and compare it with the pressure due to solar radiation. This will be done for a satellite skin of 0.79-mm-thick stainless steel. For an absorption coefficient of 0.1 and an incident irradiance of 800 W/m², about 1.9×10^{-3} cal/sec cm² are absorbed as heat. If this is assumed to be uniformly distributed through the thickness of the skin, the magnitude of the volume heat source is 2.4×10^{-2} cal/sec cm³. Since for stainless steel the density ρ is 7.93 g/cm³, and the specific heat capacity is 0.12 cal/g kelvin, the rate of temperature rise is 2.5×10^{-2} kelvin/sec. For a source half-period of 2 sec, the temperature rise is $\Delta T = 5 \times 10^{-2}$ kelvins. Inserting this in Eq. (52b) gives

$$\Delta p = 4.2 \times 10^{-5} p. \quad (52c)$$

In an environmental test chamber that can duplicate atmospheric conditions at 200 km, the pressure would be about 10^{-6} Torr, or 1.3×10^{-4} N/m². From Eq. (52c), we have $\Delta p = 5.46 \times 10^{-9}$ N/m². This is about 1/500 times the estimated light pressure of 2.6×10^{-6} N/m². According to Eq. (52c), the gas pressure could be 10 times higher and the radiometer force would still be small compared to the radiation pressure. Unfortunately, Eq. (52a) does not hold at higher pressure. A more general relation is given by Knudsen [6], but it contains four empirical constants unknown for the satellite-test chamber situation. Thus, we are probably safe only in making estimates at the lower pressure since the mean free path in that case, of the order of 60 m, is long enough to satisfy the conditions under which Eq. (52a) is derived.

SOLAR SIMULATION

The limiting accuracy in the force measurement procedure being considered is determined by the accuracy of solar simulation. The state of the art in solar simulation [7] is such that beams over 6.1 m in diameter have been projected. Beams can be made uniform to $\pm 5\%$. By filtering xenon arc lamps, we can obtain matches to the sun's spectrum above the atmosphere sufficiently good that pressure errors for the spectrum as a whole may be as low as 3.5%. Thus, the errors contributed to the measurements by the simulator should allow the force on a satellite to be measured to an accuracy of a few percent.

CONCLUSION

The analysis of this report indicates that a favorable S/N ratio for a simulation experiment could probably be achieved on a vibration isolation table in a normal laboratory environment by taking advantage of mechanical common-moding techniques. This would allow a proof-of-principle experiment to be performed that would result in experimental confirmation or rejection of the feasibility of the approach to satellite solar radiation force measurement developed here. However, before attempting to carry out force measurements on a satellite, one would require detailed information on the ambient noise spectrum in the vacuum test chamber selected for the measurements. The damping time of a large mass suspended in the same way as that contemplated for the satellite should also be measured. From this information, the S/N ratio achievable for various values of the common-mode rejection ratio could be estimated, and the overall probability of success of the measurements procedure could be predicted.

ACKNOWLEDGMENT

The author is indebted to Dr. Robert A. Masumura for a number of important discussions concerning the metallurgical ramifications of this problem during its early stages. He would also like to thank Mr. J. W. Ferguson for bringing Ref. 4, the key to the solution of the problem, to his attention, and Mr. Randolph Taylor for furnishing Ref. 8, which describes the state of the art in solar simulation. Finally, he would like to thank Dr. William H. Carter for providing assistance during the author's first experience in operating a time-shared terminal.

REFERENCES

1. R.A. Becker, *Introduction to Theoretical Mechanics*, McGraw-Hill, New York, 1954, Ch. 7 and 11.
2. I.S. Gradshteyn and I.M. Ryzhik, *Table of Integrals, Series and Products*, 4th ed., Academic Press, New York, 1965, p. 29.
3. R.W. Ditchburn, *Light*, 2d ed., Interscience, New York, 1963, Ch. 17.

4. G.R. Irwin, "Light Armor. IX, Construction and Use of Pendulums for Small Plate Testing, Brinell Hardness Correlation with Ballistic Penetration Resistance, and the Effects of Physical Defects on Armor Performance." NRL Report 1778, Sept. 4, 1941.
5. R.W. Harris, personal communication.
6. F. Garofalo, *Fundamentals of Creep and Creep-Rupture in Metals*, Macmillan Series in Materials Science, Macmillan, New York, 1965, Ch. 2.
7. M. Knudsen, *The Kinetic Theory of Gases*, 3rd ed., Methuen & Co., London, 1950, p. 52-61.
8. J.H. Beauchene and P.R. Dennis, "Simulation of the Sun," *Optical Spectra* 4 (No. 3), 48 (1970).

Appendix A

DERIVATION OF IDENTITIES FOR EQUATIONS (5a) AND (5b)

In this appendix, the identities used in Eqs. (5a) and (5b) are derived. We first compute $\sum_{\ell=0}^{n-1} \exp(\ell\theta_1) \sin \ell\theta_2$ and $\sum_{\ell=0}^{n-1} \exp(\ell\theta_1) \cos \ell\theta_2$. The procedure is to write the sine and cosine in complex form and then use the formula for the sum of a geometrical progression:

$$\begin{aligned} \sum_{\ell=0}^{n-1} e^{\ell\theta_1} \sin \ell\theta_2 &= \sum_{\ell=0}^{n-1} e^{\ell\theta_1} \left(\frac{e^{i\ell\theta_2}}{2i} - \frac{e^{-i\ell\theta_2}}{2i} \right) \\ &= \frac{1}{2i} \frac{1 - e^{(\theta_1 + i\theta_2)n}}{1 - e^{\theta_1 + i\theta_2}} - \frac{1}{2i} \frac{(1 - e^{(\theta_1 - i\theta_2)n})}{1 - e^{(\theta_1 - i\theta_2)}}. \end{aligned} \quad (\text{A1})$$

When the numerator and denominator of each term are multiplied by the complex conjugate of its denominator, this becomes

$$\frac{1}{2i(1 - e^{\theta_1} 2 \cos \theta_2 + e^{2\theta_1})} \left[-e^{\theta_1} e^{-i\theta_2} - e^{\theta_1 n} e^{i\theta_2 n} + e^{\theta_1(n+1)} e^{i\theta_2(n-1)} \right. \\ \left. e^{\theta_1} e^{i\theta_2} + e^{\theta_1 n} e^{-i\theta_2 n} - e^{\theta_1(n+1)} e^{-i\theta_2(n-1)} \right].$$

Rewriting the complex exponentials in terms of sines and cosines produces the final result:

$$\sum_{\ell=0}^{n-1} e^{\ell\theta_1} \sin \ell\theta_2 = \frac{e^{\theta_1} \sin \theta_2 - e^{\theta_1 n} \sin \theta_2 n + e^{\theta_1(n+1)} \sin \theta_2(n-1)}{1 - e^{\theta_1} 2 \cos \theta_2 + e^{2\theta_1}}. \quad (\text{A2})$$

In a similar manner, one finds that

$$\sum_{\ell=0}^{n-1} e^{\ell\theta_1} \cos \ell\theta_2 = \frac{1 - e^{\theta_1} \cos \theta_2 - e^{\theta_1 n} \cos \theta_2 n + e^{\theta_1(n+1)} \cos \theta_2(n-1)}{1 - e^{\theta_1} 2 \cos \theta_2 + e^{2\theta_1}}. \quad (\text{A3})$$

Using Eqs. (A2) and (A3), we may compute the sums $\sum_{\ell=0}^{n-1} \exp(\ell\theta_1) \cos(\ell\theta_2 + \phi)$ and $\sum_{\ell=0}^{n-1} \exp(\ell\theta_1) \sin(\ell\theta_2 + \phi)$. From the trigonometric identities for the sum of two angles, we have

$$\begin{aligned} \sum_{\ell=0}^{n-1} e^{\ell\theta_1} \sin(\ell\theta_2 + \phi) &= \sum_{\ell=0}^{n-1} e^{\ell\theta_1} (\sin \ell\theta_2 \cos \phi + \cos \ell\theta_2 \sin \phi) \\ &= \cos \phi \sum_{\ell=0}^{n-1} e^{\ell\theta_1} \sin \ell\theta_2 + \sin \phi \sum_{\ell=0}^{n-1} e^{\ell\theta_1} \cos \ell\theta_2. \end{aligned}$$

By substituting the previously computed expressions for the sums, one immediately has

$$\begin{aligned} \sum_{\ell=0}^{n-1} e^{\ell\theta_1} \sin(\ell\theta_2 + \phi) &= \cos \phi \left[\frac{e^{\theta_1} \sin \theta_2 - e^{\theta_1 n} \sin \theta_{2n} + e^{\theta_1(n+1)} \sin \theta_{2(n-1)}}{1 - e^{\theta_1} 2 \cos \theta_2 + e^{2\theta_1}} \right] \\ &+ \sin \phi \left[\frac{1 - e^{\theta_1} \cos \theta_2 - e^{\theta_1 n} \cos \theta_{2n} + e^{\theta_1(n+1)} \cos \theta_{2(n-1)}}{1 - e^{\theta_1} 2 \cos \theta_2 + e^{2\theta_1}} \right]. \end{aligned}$$

In a similar fashion, one finds that

$$\begin{aligned} \sum_{\ell=0}^{n-1} e^{\ell\theta_1} \cos(\ell\theta_2 + \phi) &= \cos \phi \left[\frac{1 - e^{\theta_1} \cos \theta_2 - e^{\theta_1 n} \cos \theta_{2n} + e^{\theta_1(n+1)} \cos \theta_{2(n-1)}}{1 - e^{\theta_1} 2 \cos \theta_2 + e^{2\theta_1}} \right] \\ &- \sin \phi \left[\frac{e^{\theta_1} \sin \theta_2 - e^{\theta_1 n} \sin \theta_{2n} + e^{\theta_1(n+1)} \sin \theta_{2(n-1)}}{1 - e^{\theta_1} 2 \cos \theta_2 + e^{2\theta_1}} \right]. \end{aligned}$$